Landsvirkjun

LV-2022-027

2021 GNSS surveying and surface deformation at Krafla, Námafjall and Þeistareykir

Status Report, February 2022

2021 GNSS surveying and surface deformation at Krafla, Námafjall and Þeistareykir

Status Report, February 2022

Höfundar
Chiara Lanzi [1], Freysteinn Sigmundsson [1],
Halldór Geirsson [1], Sigrún Hreinsdóttir[2]
(1) Nordic Volcanological Center, Institute of Earth Sciences,
University of Iceland
(2) GNS Science, Lower Hutt, New Zealand
Science Institute report RH-2-22

Dagsetning
April 2022

Lykilsíða

Skýrsla LV nr	LV-2022-027	**Dagsetning**	April 2022
Fjöldi Síðna	49	**Upplag**	1
Dreifing	[ ] Birt á vef LV	[X] Opin	[ ] Takmörkuð til [Dags.]
Titill	2021 GNSS surveying and surface deformation at Krafla, Námafjall and Þeistareykir. Status Report, February 2022		
Höfundar/fyrirtæki	Chiara Lanzi, Freysteinn Sigmundsson, Halldór Geirsson, Sigrún Hreinsdóttir		
Verkefnisstjóri	Anette Kærgaard Mortensen		
Unnið fyrir	Landsvirkjun		
Samvinnuaðilar	–		
Útdráttur	We report on GNSS surveying carried out in Krafla, Námafjall and Þeistareykir areas in the summer of 2021. An overview of the measurements is provided, followed by results showing times series of ground displacements and vector displacements. Geodetic modelling is also provided. The analysis of GNSS time series helps to define the temporal and spatial evolution of the deformation. At Krafla, deformation patterns changed in the middle of 2018. Difference of velocity fields prior to and after 2018 reveal inflation pattern at rate of few mm/yr; observed in the caldera for the first time since 1989. After an initial faster deformation phase (fall 2018 - end 2019), the deformation rate was less in 2020. The responsible process may continue at present. The maximum deformation area is localized in the middle of the caldera, between Leirhnjúkur and the IDDP-1 well. Modelling of the inflation deformation favours a point source of pressure model at 2.1– 2.8 km depth, centred ~0.5 km north-west to the IDDP-1 borehole. The GNSS time series analysis carried out in Þeistareykir area shows no significant deformation, except for a localized area north-west of Bæjarfjall, up to 2-3 mm/yr of subsidence.		
Lykilorð	GNSS surveying, GNSS time series, deformation, Krafla, Námafjall, Þeisatreykir, geothermal field, 2021		

Samþykki verkefnisstjóra Landsvirkjunar

Anette K. Mortensen

Table of contents

List of figures

Figure 15. GNSS time series for THRC GNSS station analysed by Sigrún Hreinsdóttir with GAMIT-GLOBK software.

Figure 16. Upper panel, map for the GNSS time series being shown figures 16 (lower panel), 17 and 18. Lower panel, GNSS time series for TRG2 station at Þeistareykir.
Figure 17. GNSS time series for TH17 station at Þeistareykir.

Figure 18. 2018-2021 horizontal GNSS velocities relative to the stable Eurasian plate, in the Krafla and Námafjall areas. Blue triangles show the campaign GNSS stations, while the red ones show the continuous stations. Ellipses indicate velocity uncertainties.

Figure 19. 2018-2021 Vertical (right) GNSS velocities in the Krafla and Námafjall areas. Blue triangles show the campaign GNSS stations, while the red ones show the continuous stations. Ellipses indicate velocity uncertainties.

Figure 20. Horizontal velocity field 2018-2020 relative to 2015-2018 in the Krafla area. Blue triangles show the campaign GNSS station, while the red ones show the continuous station. Ellipses indicate velocity uncertainties.

Figure 21. Vertical velocity field 2018-2020 relative to 2015-2018 in the Krafla area. Blue triangles show the campaign GNSS station, while the red ones show the continuous station. Ellipses indicate velocity uncertainties.

Figure 22. Horizontal velocity field 2018-2021 relative to 2015-2018 in the Krafla area. Blue triangles show the campaign GNSS station, while the red ones show the continuous station. Ellipses indicate velocity uncertainties.

Figure 23. Vertical velocity field 2018-2021 relative to 2015-2018 in the Krafla area. Blue triangles show the campaign GNSS station, while the red ones show the continuous station. Ellipses indicate velocity uncertainties.

Figure 24. Horizontal (upper left panel) and vertical (lower left panel) difference velocity field 2018-2020 relative to 2015-2018 in the Krafla area. Horizontal (upper right panel) and vertical (lower right panel) difference velocity field 2018-2021 relative to 2015-2018 in the Krafla area. Blue triangles show the campaign GNSS station, while the red ones show the continuous station. Ellipses indicate velocity uncertainties.

Figure 25. 2017-2021 horizontal GNSS velocities relative to 2015-2017 in Þeistareykir area. Blue triangles show the campaign GNSS station, while the red ones show the continuous station.

List of tables

SUMMARY

We report GNSS surveying carried out in Krafla, Námafjall and Þeistareykir areas in the summer of 2021. An overview of the measurements is provided, followed by results showing times series of ground displacements and vector displacements. Geodetic modelling is also provided. The analysis of GNSS time series helps to define the temporal and spatial evolution of the deformation. At Krafla, deformation patterns changed in the middle of 2018. Difference of velocity fields prior to and after 2018 reveal inflation pattern at rate of few mm/yr; observed in the caldera for the first time since 1989. After an initial faster deformation phase (fall 2018 - end 2019), the deformation rate was less in 2020. The responsible process may continue at present. The maximum deformation area is localized in the middle of the caldera, in-between Leirhnjúkur and the IDDP-1 well. Modelling of the inflation deformation favours a point source of pressure model at 2.1– 2.8 km depth, centred ~0.5 km north-west to the IDDP-1 borehole. The GNSS time series analysis carried out in Þeistareykir area shows no significant deformation, except for a localized area north-west of Bæjarfjall, up to 2-3 mm/yr.

1. GNSS MEASUREMENTS

Global Navigation Satellite Systems (GNSS) use constellations of satellites orbiting over the Earth's surface, transmitting signals that enable users to determine their position and perform accurate geodetic measurements. One of the satellite constellations is the Global Positioning System (GPS). GNSS equipment produced in recent years can typically track signals from other networks additional to the GPS system, and therefore the measurements are referred to as GNSS-measurements. More satellites generally result in increased accuracy of geodetic measurements.

A dense network with more than 90 GNSS sites has been established through the years to monitor the ground deformation at Krafla, Námafjall and Þeistareykir areas (Figures 1 and 2). Data processing so far have only utilized signals from the GPS system. The network consists of continuous GNSS stations (Table 1) and stations occupied during campaign measurements (Figure 3). Campaign sites are typically occupied for one or several days to achieve sufficient accuracy.

GNSS measurements in 2021 (Appendix A) were planned to optimize the spatial coverage of the areas of highest interest. Length and quality of time series from data collected in previous surveys and geodetic monument stability was also taken into consideration when selecting sites to measure in 2021.

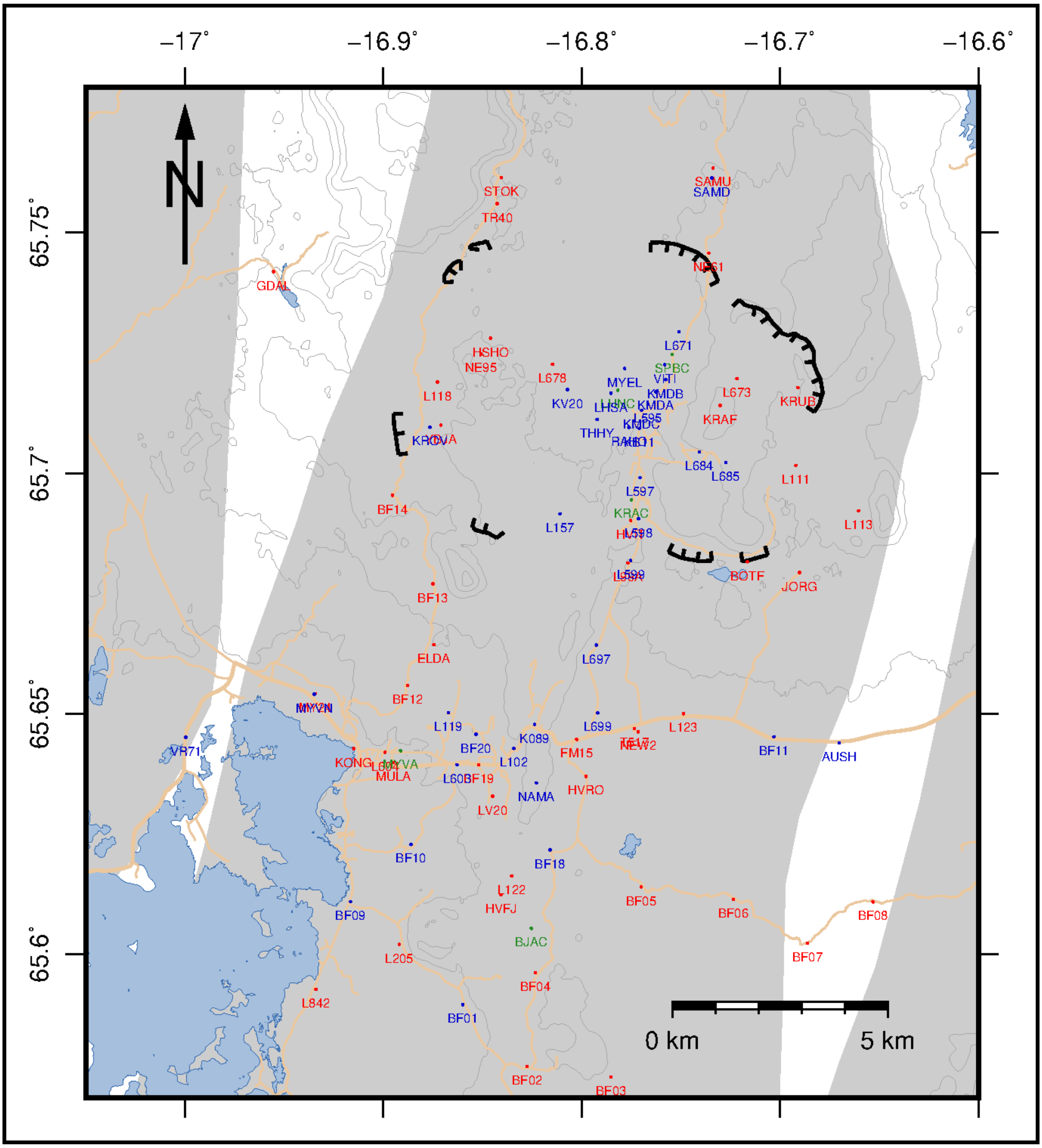

Figure 1. GNSS stations in the Krafla and Námafjall area in 2021. Continuous stations are shown with a green label, campaign sites measured in 2021 with a blue label. Stations with a red label have been measured in earlier years, but not in 2021.

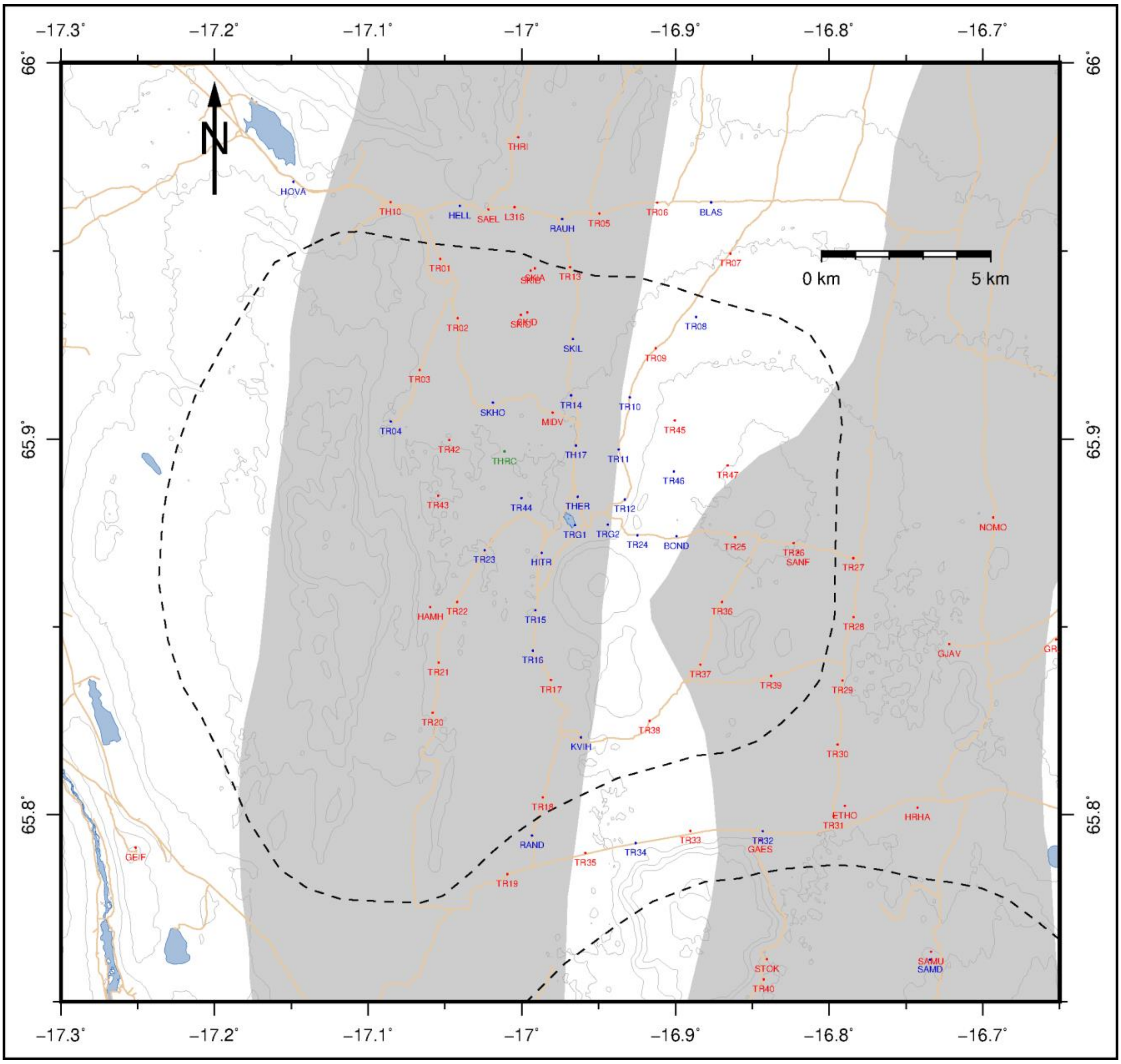

Figure 2. GNSS stations in Þeistareykir area in 2021. Continuous stations are shown with a green label, campaign sites measured in 2021 with a blue label. Stations with a red label have been measured in earlier years, but not in 2021.

Table 1. Continuous GNSS sites.

Location	Station name	Start of recording
Krafla	KRAC	2011
Krafla	LHNC	November 2019
Krafla	SPBC	November 2019
Námafjall	BJAC	2012
Mývatn	MYVA	2006
Þeistareykir	THRC	2011

Figure 3. GNSS measurements. Left: a continuous GNSS site (KRAC), which collects data night and day for long times. Right: GNSS temporary set-up of equipment during campaign measurements (shorter time, typically several days, for each single GNSS site).

1.1 Equipment and measurements

GNSS receivers for the 2021 campaign measurements were configured to sample appropriate satellite data every 15 seconds. Each campaign GNSS station was occupied for at least 48 hours. Instruments used for the measurements were from the Institute of Earth Sciences (IES) at University of Iceland, and King Abdullah University of Science and Technology (KAUST). Receiver types used in this campaign were: Trimble 5700, Septentrio PolarX5 and NetR9. The antenna type used in the 2021 campaign is: Trimble Zephyr Geodetic (TRM41249.00 and TRM57971.00).

Measurement accuracy is related to the quality of the tripod and antenna set and its stability during observations. Antennas need to be precisely centred and levelled above the geodetic benchmark on the ground, and the antenna height needs to be carefully measured. We measured the slant antenna height (the distance from the benchmark on the ground to the bottom edge of the antenna) both in meters and feet, for redundancy (Appendix B). The slant height is then changed into vertical height when data is prepared for analyses. It is best practice to orient each antenna in the same geographic direction. In our case all the antennas have been aligned to the true north, using a compass with 13 degrees magnetic declination. Antennas are installed on a tribrach fastened to a tripod, ensuring their centring over the benchmark on the ground. The antenna height and centring, as well as level of the antenna are checked at the beginning and end of each measurement.

For each GNSS site we fill out a log-sheet form. This document includes all relevant information regarding the occupation, such as: observer, session start and end of recording, receiver and antenna serial numbers, antenna height at the beginning and end of the survey. An example of a log-sheet form is shown in Appendix C.

All the continuous GNSS sites were operating during the time of the 2021 campaign survey.

2. DATA ANALYSIS

2.1 Data collection

The data recorded by the receivers were downloaded in the field after a quick quality check. Data processing typically requires internet to access continuous station data, precise satellite orbits, and other detailed information for the processing. Several organizations provide precise satellite orbital information, which is calculated daily and available with a two-week delay. The use of this information (rather than the orbital information broadcast by the satellites) improves accuracy of station coordinate solutions significantly.

The raw data files are translated into so-called RINEX (Receiver Independent Exchange) format, prior to be read into the most used processing software (Gurtner, 2007). The translation, editing and quality check of the data has been made with the TEQC software (Estey et al., 1999).

2.2 Data processing

The RINEX files for campaign sites were analysed at the University of Iceland with the GAMIT-GLOBK software (Herring et al., 2010a; Herring et al., 2010b). The resulting time series were then analysed with Tsview software (Herring and McClusky, 2009). Site positions were evaluated in the ITRF2014 reference frame using over 100 worldwide reference stations. The data were corrected for ocean tidal loading using the FES2004 model (Lyard et al., 2006). The time-series were corrected for the velocity of stable Eurasian plate using the GAMIT-GLOBK software, based on the ITRF2008 plate motion model (Altamimi et al., 2012).

The GAMIT software consists of a collection of programs used for the analysis of GPS data. It uses the GPS carrier phase and pseudorange observables to estimate three-dimensional relative positions of ground stations and satellite orbits, atmospheric delays, and earth orientation parameters. The GLOBK software utilizes a Kalman filter which primary purpose is to combine various geodetic solutions. It accepts as data, or "quasi-observations" the estimates and covariance matrices for station coordinates, earth-orientation parameters, orbital parameters, and source positions generated from the analysis of the primary observations. The GAMIT-GLOBK software analysis has been developed by MIT, Scripps Institution of Oceanography and Harvard University with support from the National Science Foundation.

The processing for KRAC continuous station has been made with both GAMIT-GLOBK software (by Sigrún Hreinsdóttir), and with GIPSY-OASIS II software (Zumberge et al., 1997) by Halldór Geirsson. Both solutions are shown here, to ensure consistency of the evolution of the signals observed. The LHNC and SPBC continuous sites have been processed only with GIPSY-OASIS II software. GIPSY-OASIS II is an automated, fast, ultra-precise high precision GPS data processing software package with strict data quality control developed by the Jet Propulsion Laboratory in California.

2.3 Krafla time series

The time series for the KRAC GNSS station is shown in Figure 4 and 5. It is detrended by removing a constant trend, as well as annual and semi-annual variations in both time-series from processing with GAMIT-GLOBK and GIPSY-OASIS II. The two solutions agree quiet well with some minor deviations.

Following steady movement prior to middle of 2018, except for minor changes in relation to the 2014 Bardarbunga dike propagation and eruption, both time series show a southward movement beginning in fall 2018 and continuing to present. In fall 2018 to 2020, the analyses indicate an initial faster southern movement which subdued at the beginning of 2020 and keeps at constant rate until the end of 2021. The vertical component of both time series agree in showing a delayed upward movement at the end of 2019, compared to the onset of the southern motion that began in fall 2018. In 2021, this motion has slowed down.

In summary, the time series show a similar pattern, and local changes between the two time series are so small that they may result from the different processing approaches.

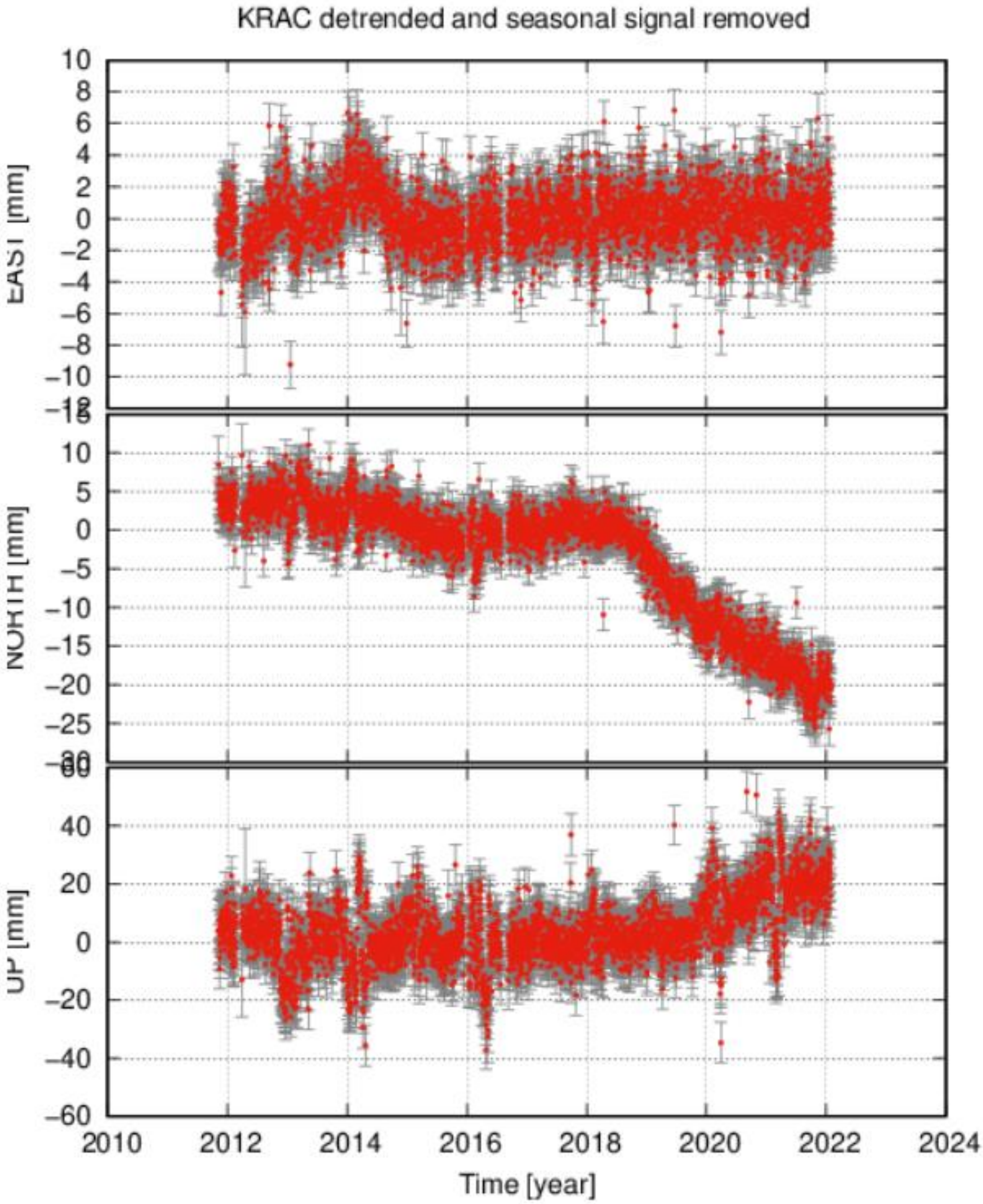

Figure 4. GNSS time series for KRAC GNSS station at Krafla as analysed by Halldór Geirsson with GIPSY-OASIS II software.

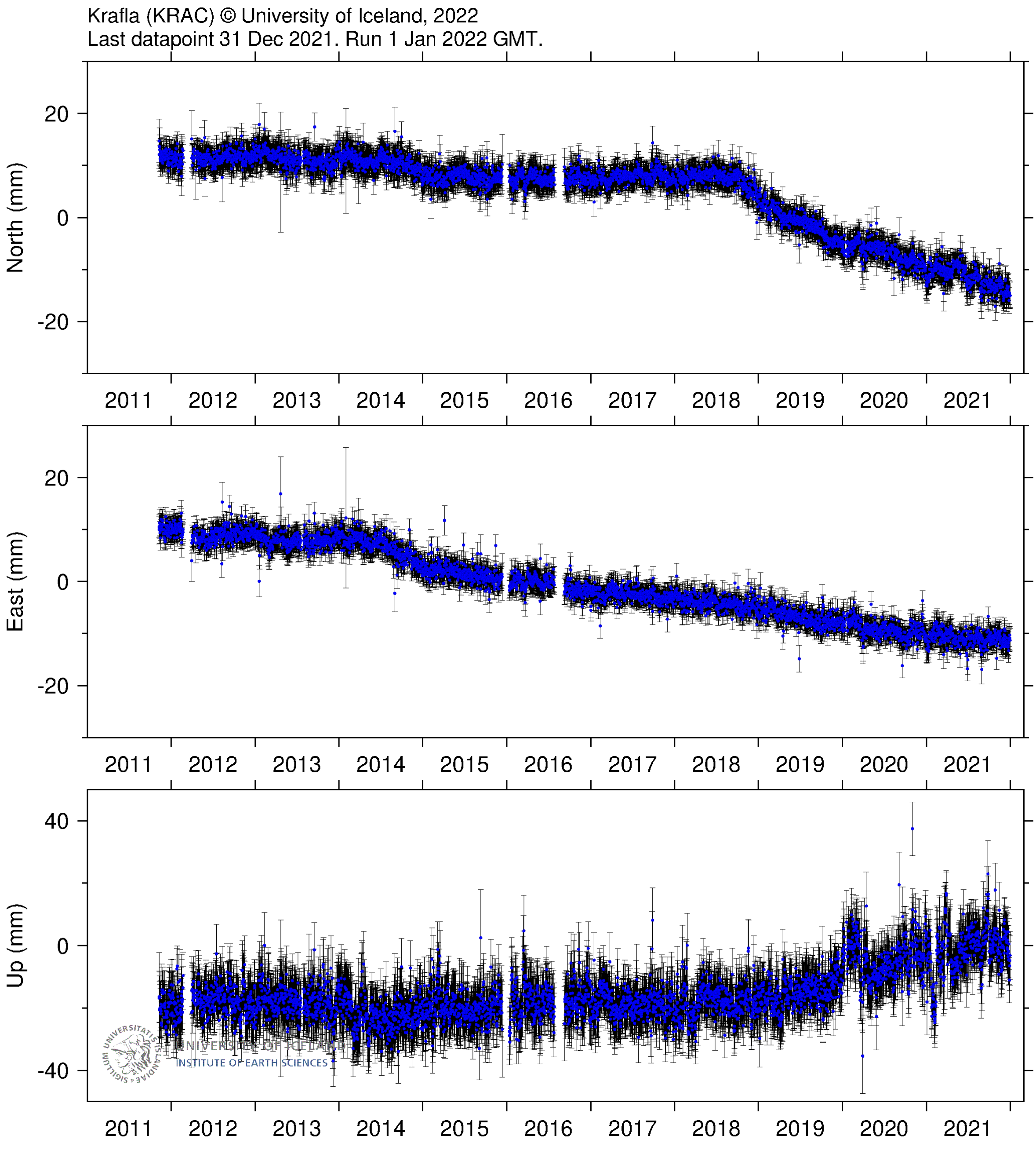

Figure 5. GNSS time series for KRAC GNSS station at Krafla as analysed by Sigrún Hreinsdóttir with GAMIT-GLOBK software.

Time series for the LHNC and SPBC continuous stations (Figures 6 and 7) are detrended for only linear variations, as the time series for these two stations are too short to estimate their seasonal signal. In addition, a part of the 2020 data for the LHNC time series has been removed due to major perturbations during the time span not shown. The most probable cause is presence of a thick snow cover; the station's antenna was buried completely by snow. The winter of 2021 also shows clear signs of perturbations caused by snow, especially in the vertical component of LHNC (Figure 7).

The observations suggest that both LHNC and SPBC sites have moved at relatively steady rates since their installation in late 2019.

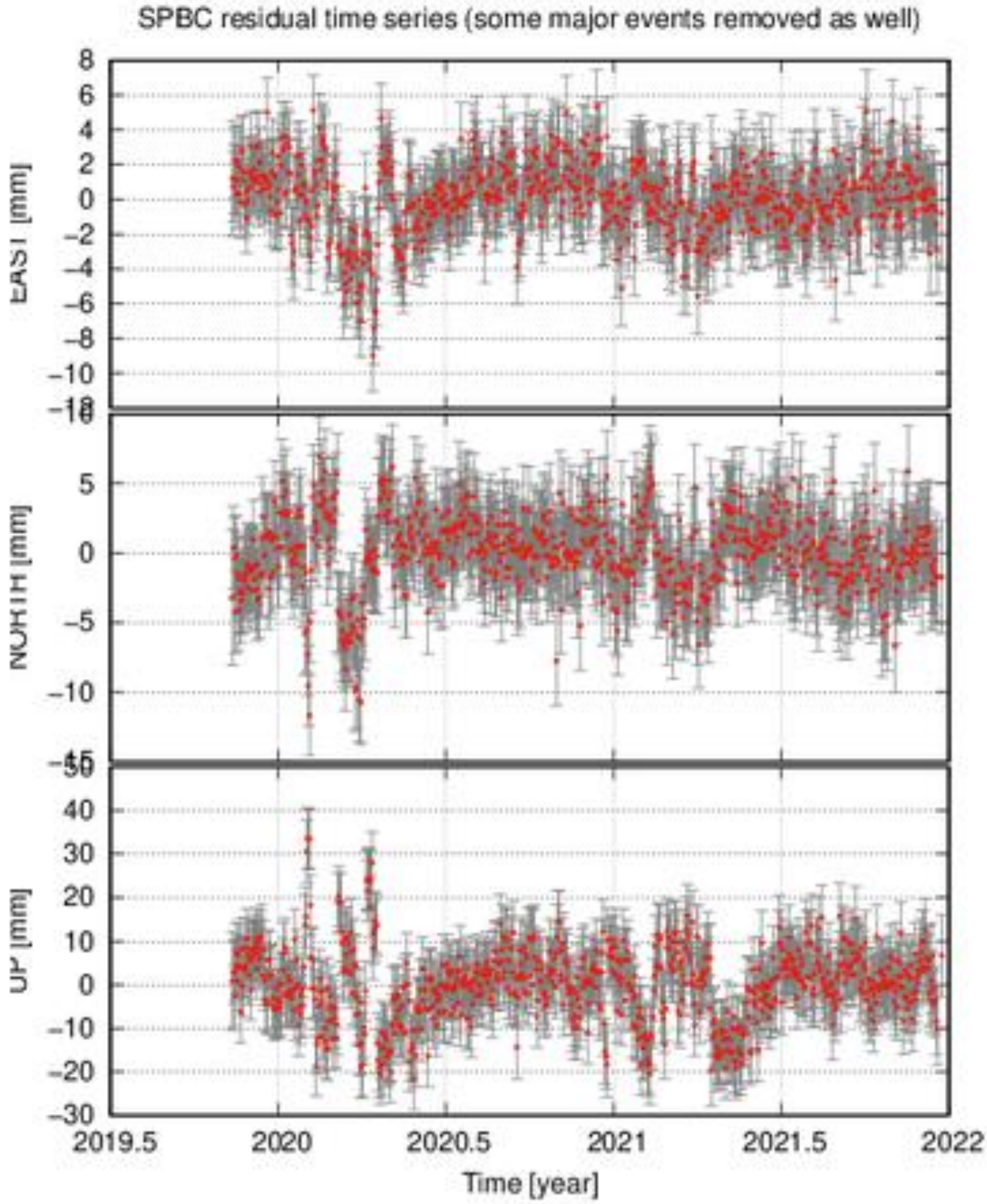

Figure 6. GNSS time series for SPBC GNSS station at Krafla as analysed by Halldór Geirsson GIPSY-OASIS II software. Displacements are detrended for linear variations in the ITRF2014.

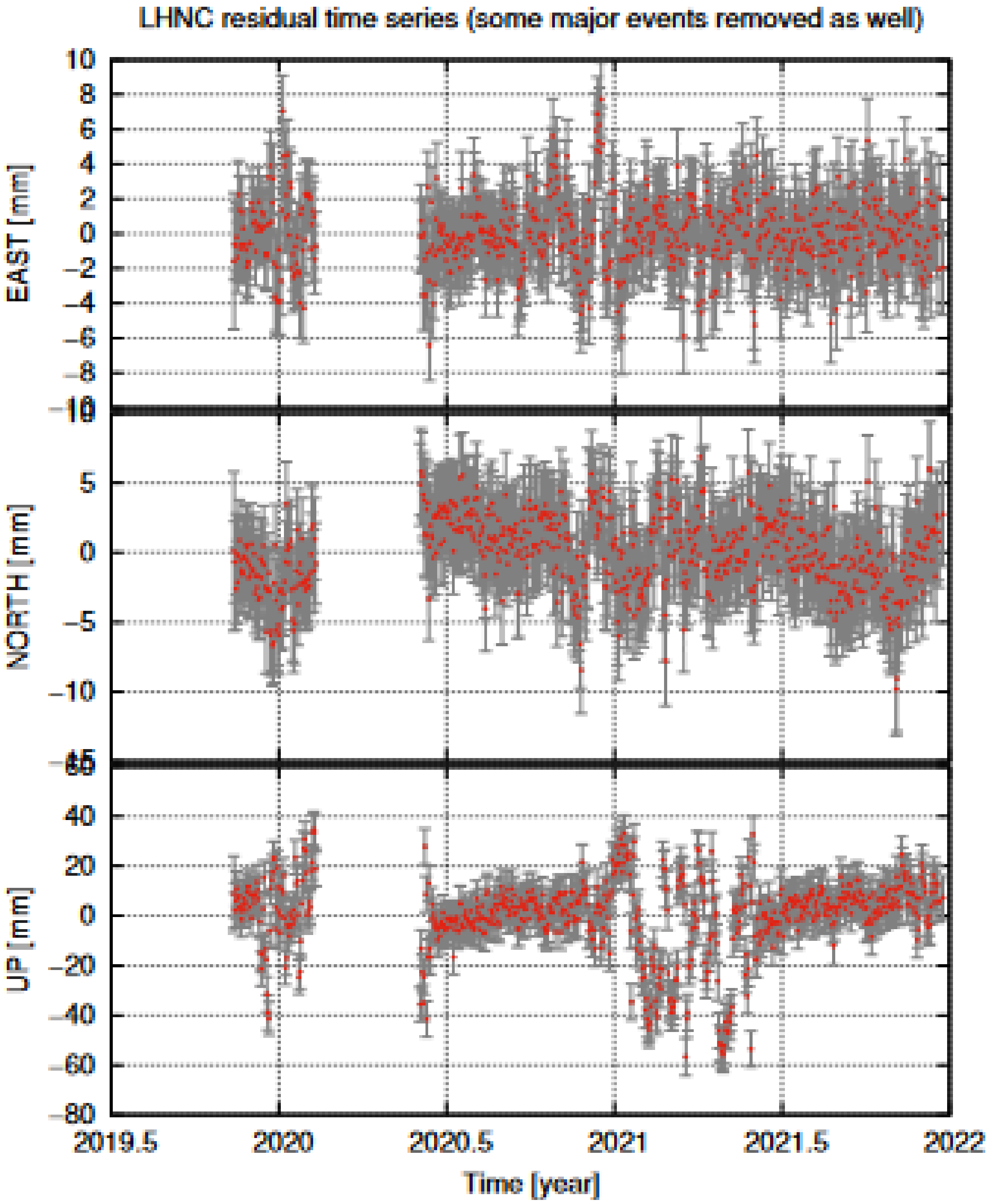

Figure 7. GNSS time series for LHNC GNSS station at Krafla as analysed by Halldór Geirsson GIPSY-OASIS II software. Displacements are detrended for linear variations in the ITRF2014.

In the following we show times series of some selected campaign GNSS stations that give further indications of the temporal history of deformation. The stations have been measured yearly since 2012 (Figures 8 - 13). The inferred north movement is rather regular in all the time series being shown. On the other hand, clear changes occur in the east component of VITI (Figure 8), L595 (Figure

8) and THHY (Figure 10) stations where the station move along a different trend after the 2018 measurements. The change is present also in the KB11 (Figure 11) and L684 (Figure 12) stations but seems delayed in the July (for KB11) and November 2019 measurement (for L684). L157 station has not been measured in 2018 but does not seem to show any significant change after 2018. Even though, the up component is noisier than the horizontal components, in all the time series is clear a change in the motion before and after 2018. All the time series shown in Figurs 8-13 are in the ITRF2014 reference frame.

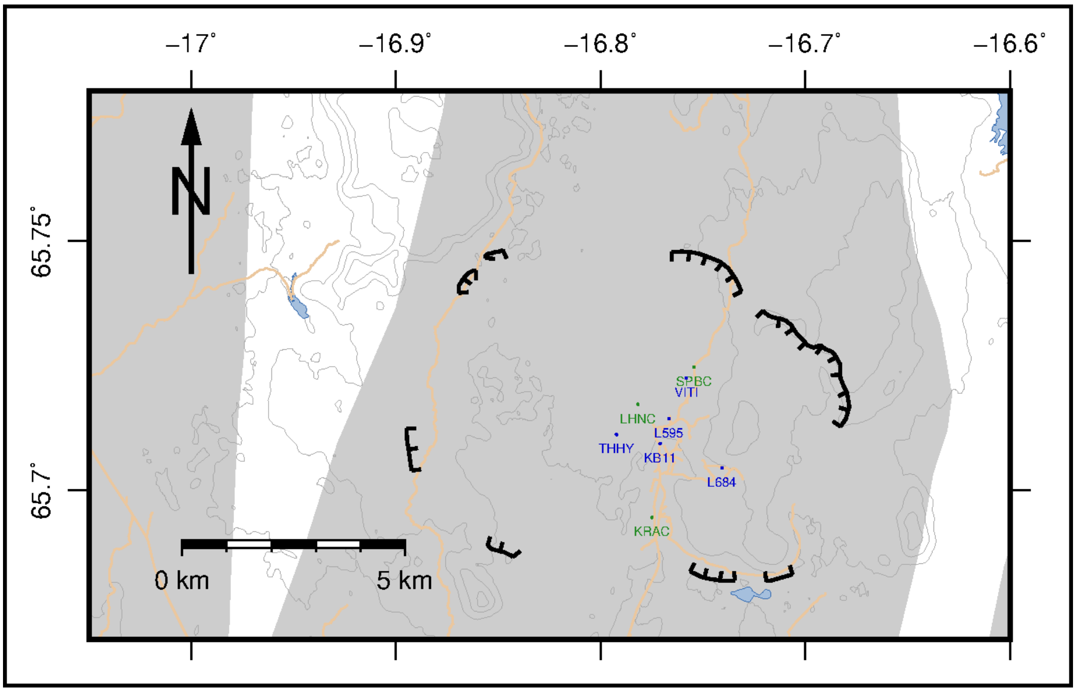

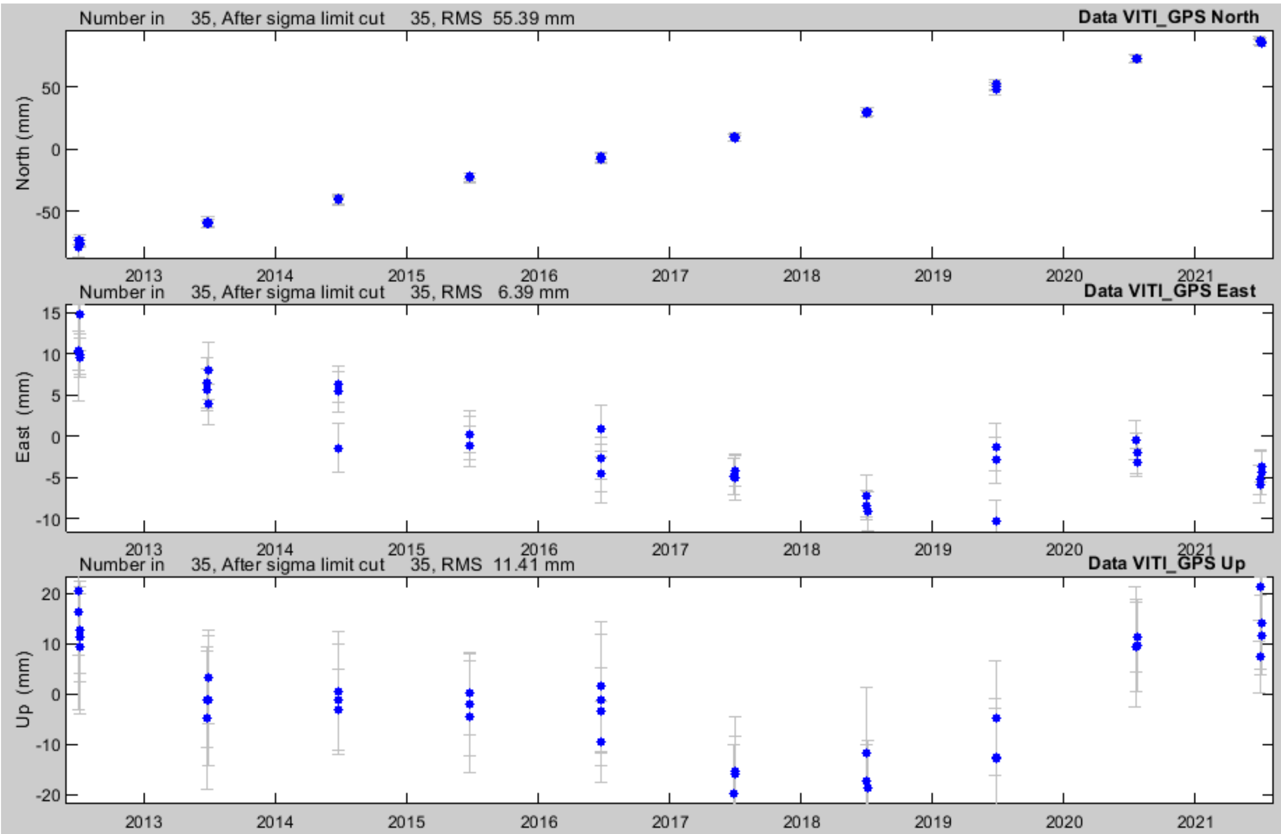

Figure 8. Upper panel, map for the GNSS time series being shown in Figures 8 (lower panel), 9, 10, 11, 12 and 13. Lower panel, time series for station VITI.

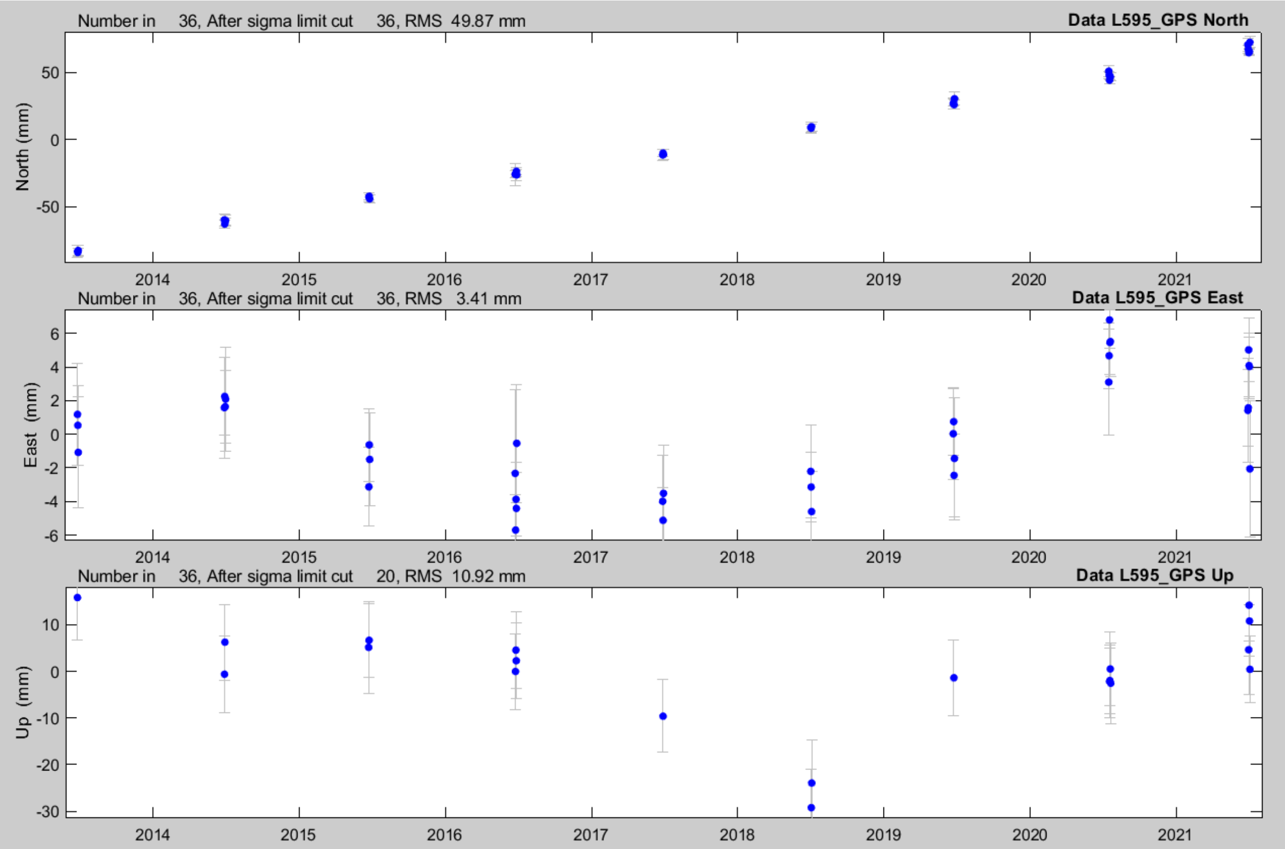

Figure 9. Time series for station L595.

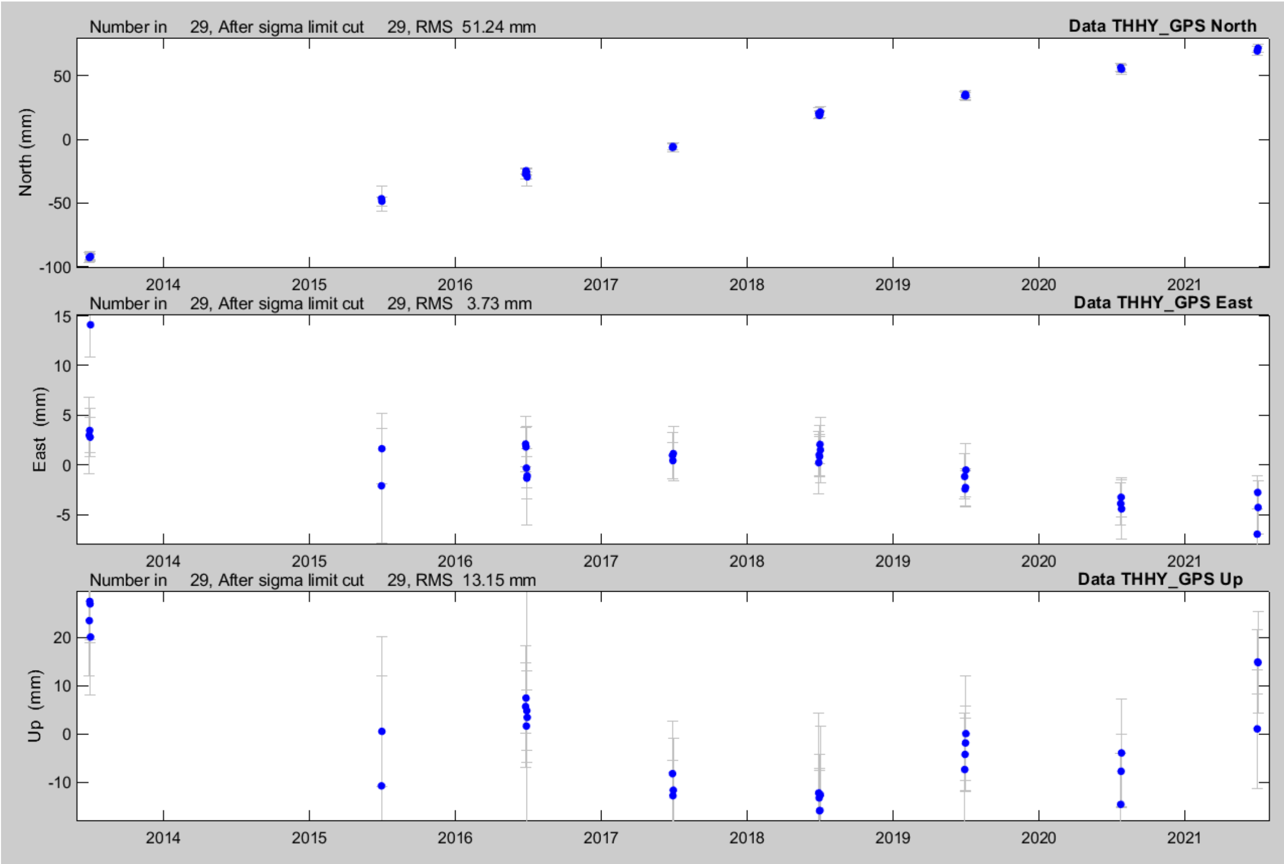

Figure 10. Time series for station THHY.

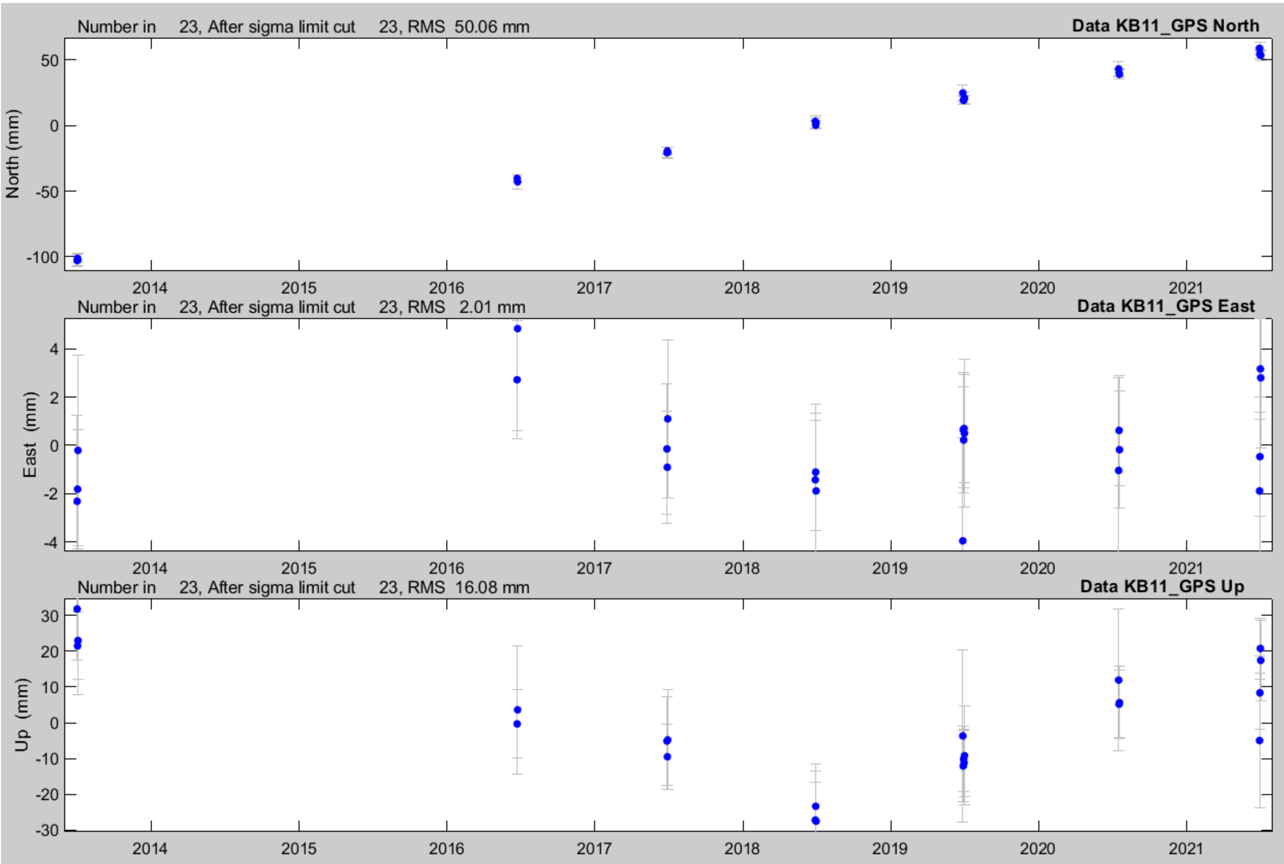

Figure 11. Time series for station KB11.

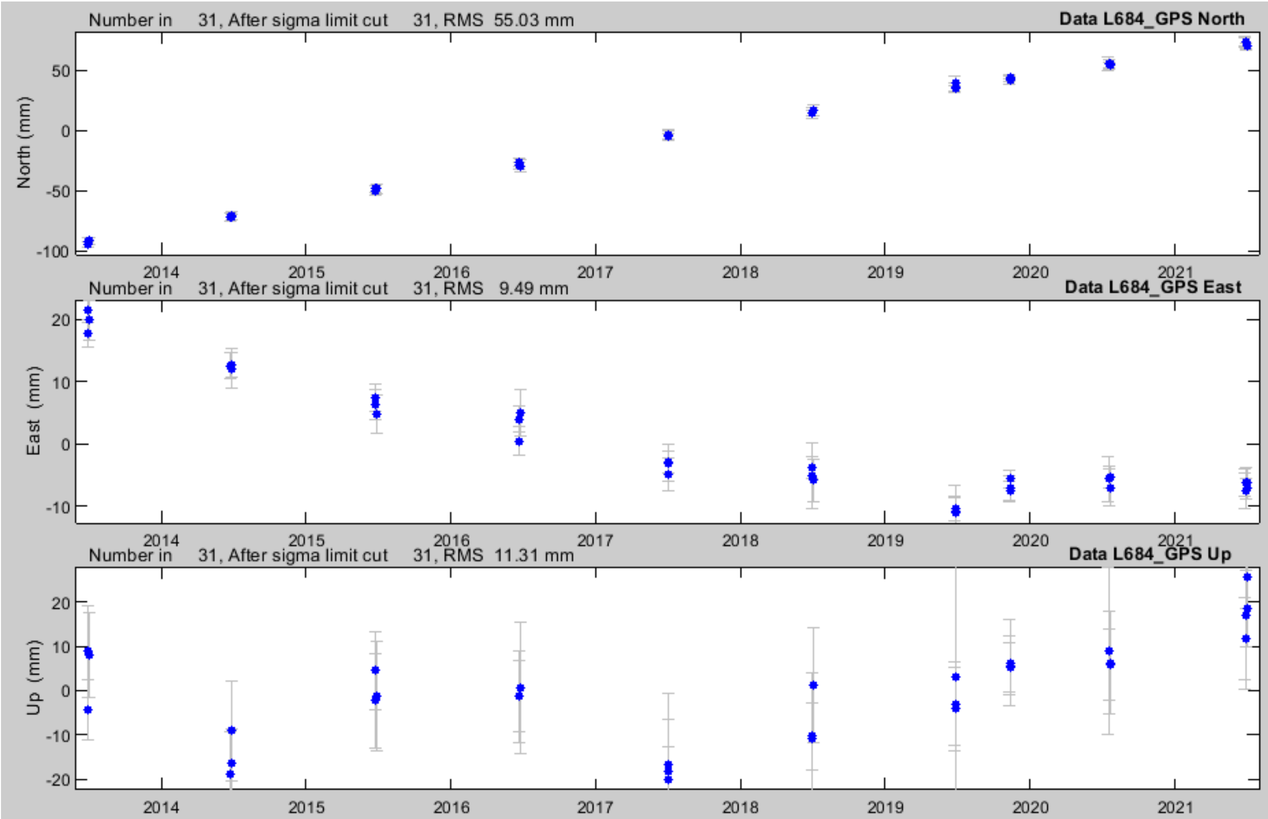

Figure 12. Time series for station L684.

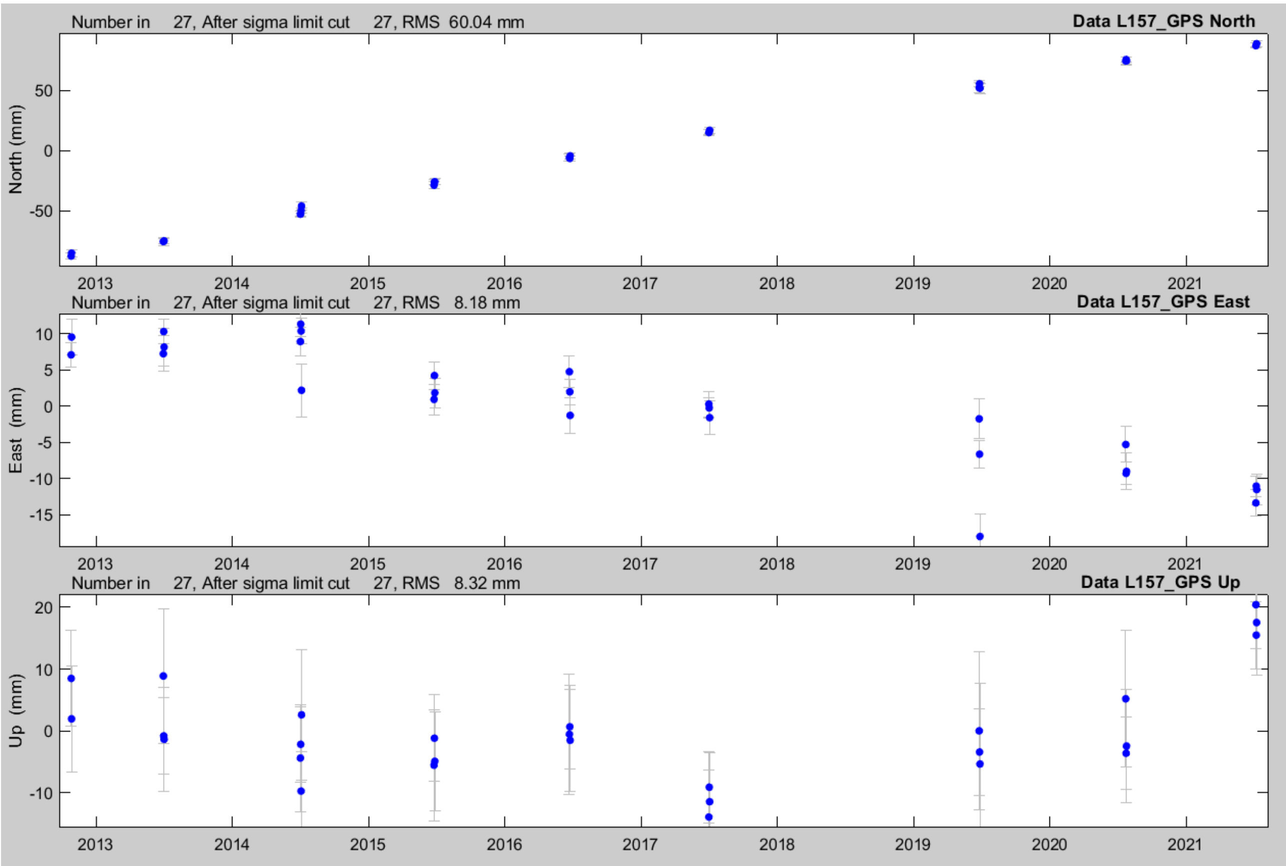

Figure 13. Time series for station L157.

2.4 Þeistareykir time series

The time series of the continuous GNSS station THRC in Þeistareykir (Figure 14) is detrended, as well as corrected for annual and semi-annual variations. In Figures 14 and 15 we present the time series for THRC according to two different processing software, GAMIT-GLOBK and GIPSY-OASIS II. Both processing solution show no significant changes and the time series show rather stable movements.

The north component is rather constant throughout the whole time series in both processing approaches. The small movement towards east started in 2019 and visible in the GIPSY-OASIS II processing, not so clear in the GAMIT-GLOBK solution, seems to have slowed down or stopped.

The up component is rather constant or slightly moving upwards according to the GIPSY-OASIS II solution. The GAMIT-GLOBK solution show a slight increase since beginning 2021.

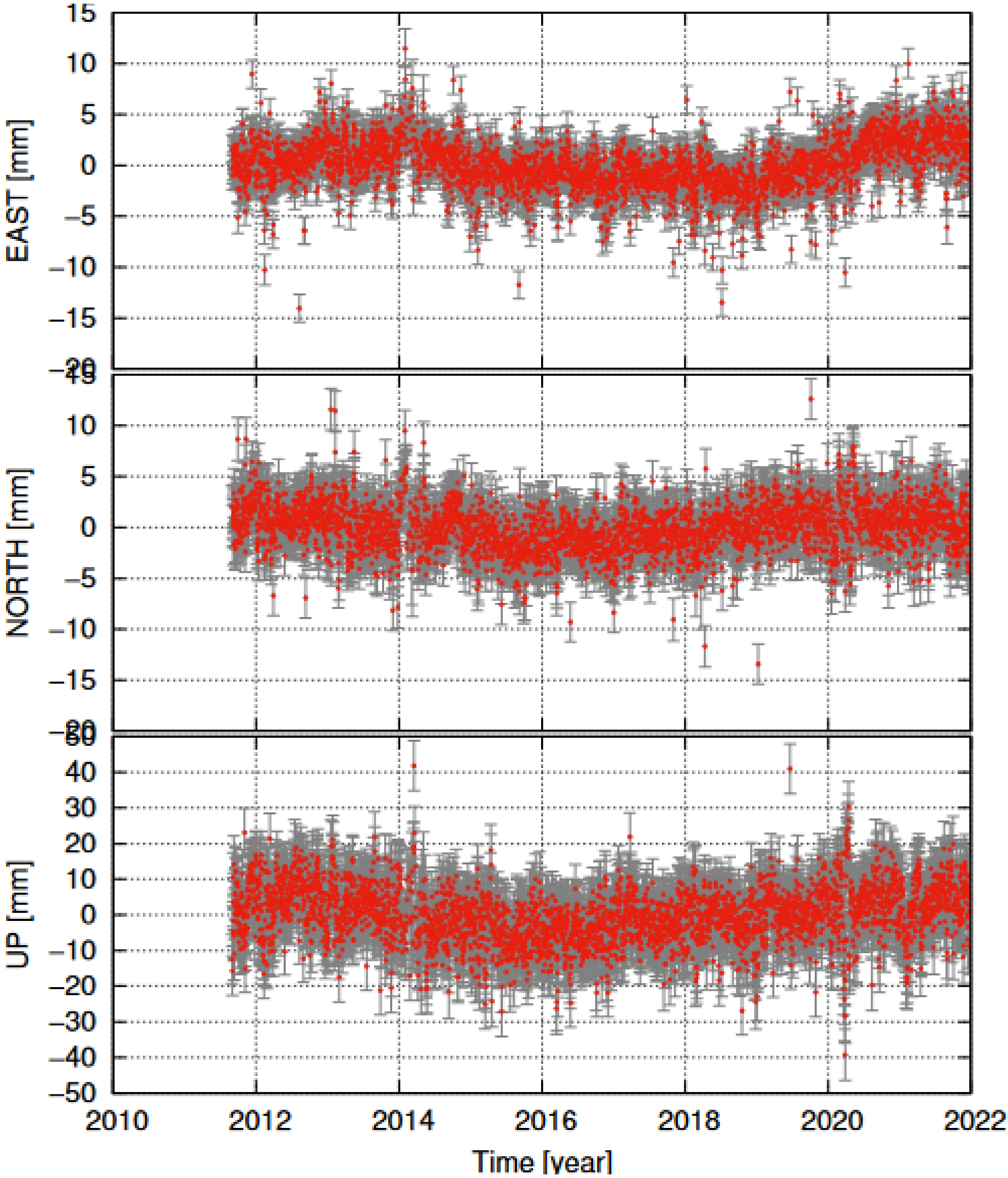

Figure 14. GNSS time series for THRC GNSS station at Krafla as analysed by Halldór Geirsson with GIPSY-OASIS II software.

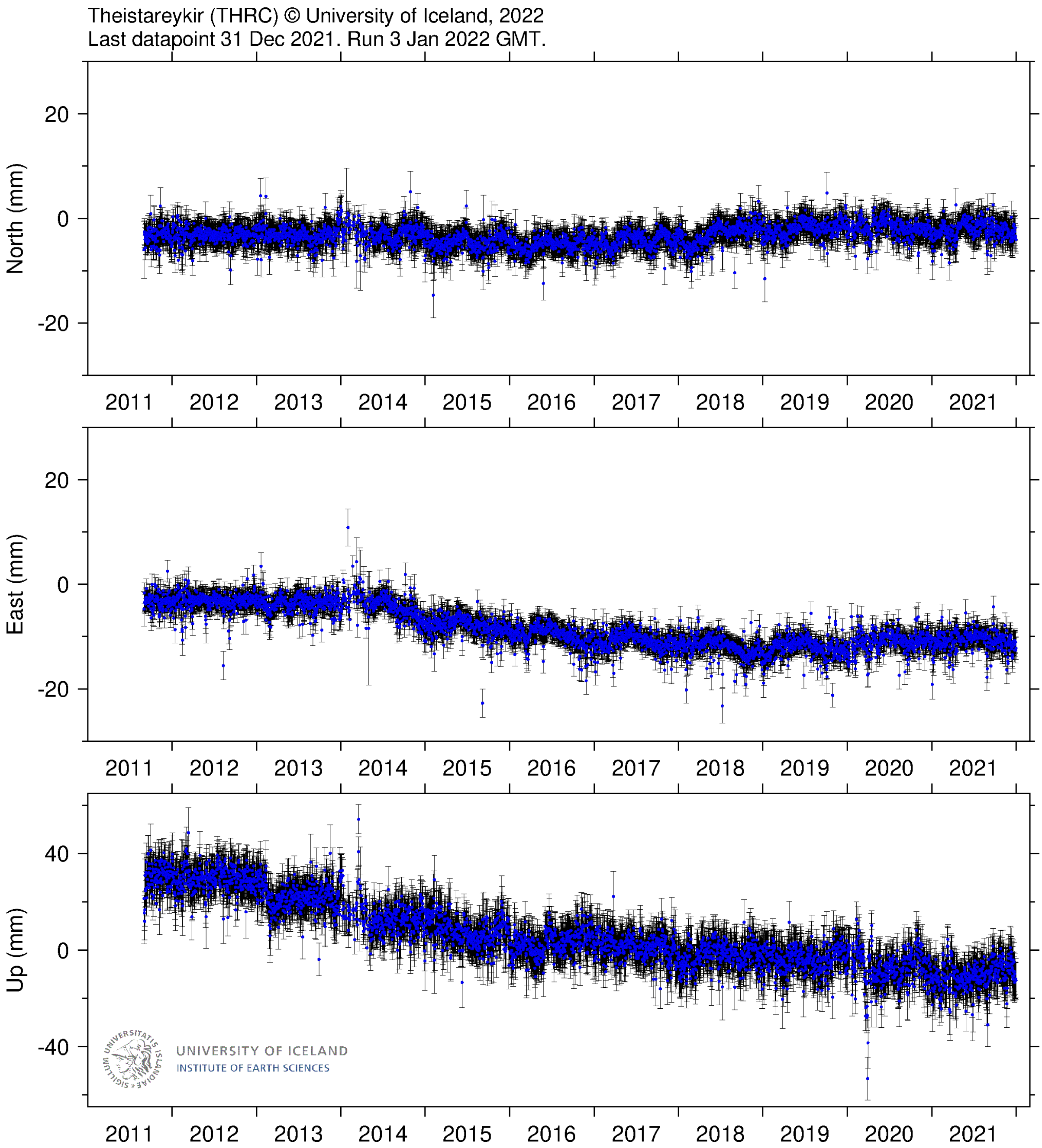

Figure 15. GNSS time series for THRC GNSS station analysed by Sigrún Hreinsdóttir with GAMIT-GLOBK software.

In Figures 16 and 17, we present some time series of the campaign GNSS sites. The horizontal motion is steady. Station TH17 gives an indication for a change in the vertical component for the past two years but the data are noisy.

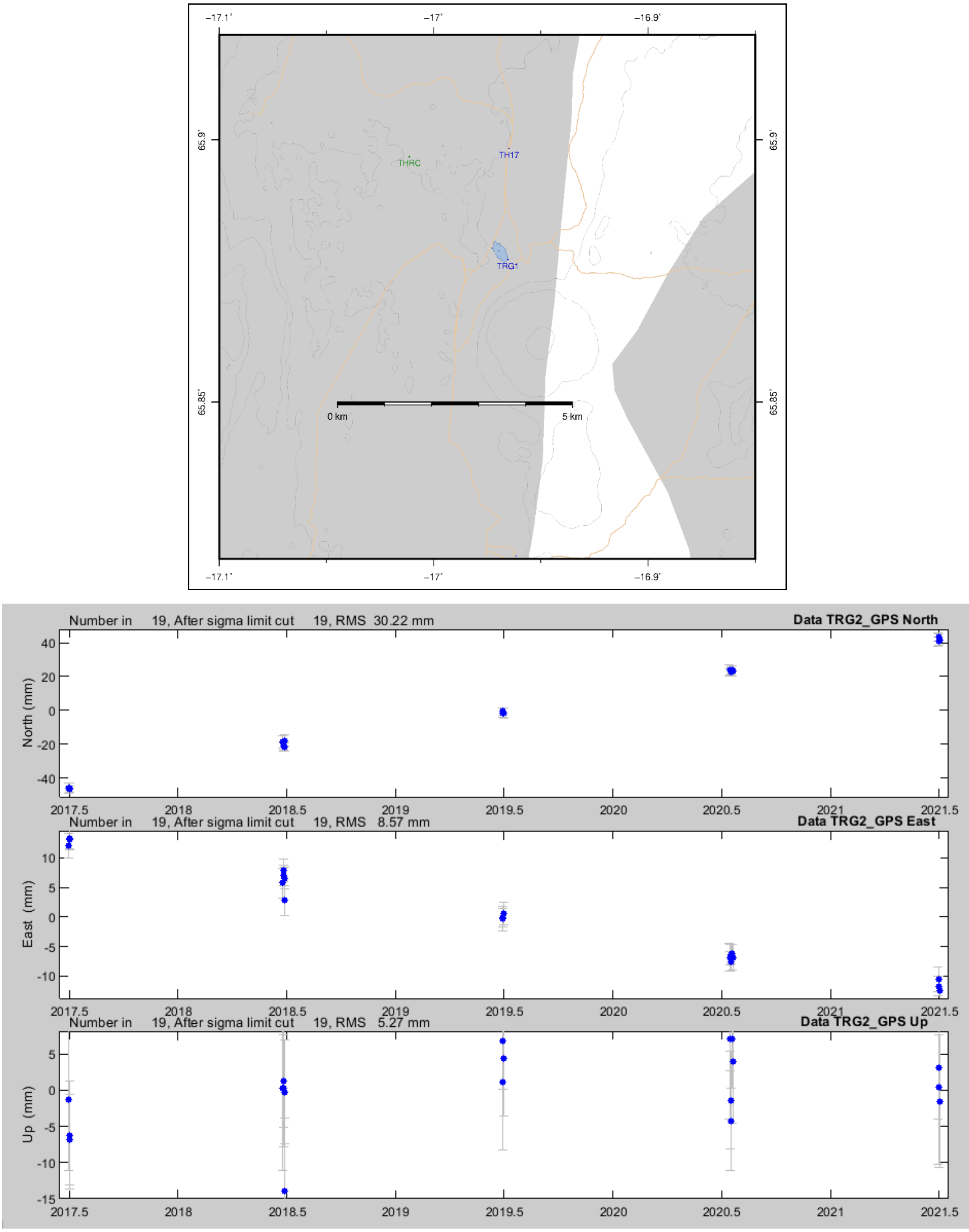

Figure 16. Upper panel, map for the GNSS time series being shown in Figures 16 (lower panel) and 17. Lower panel shows GNSS time series for TRG2 station at Þeistareykir.

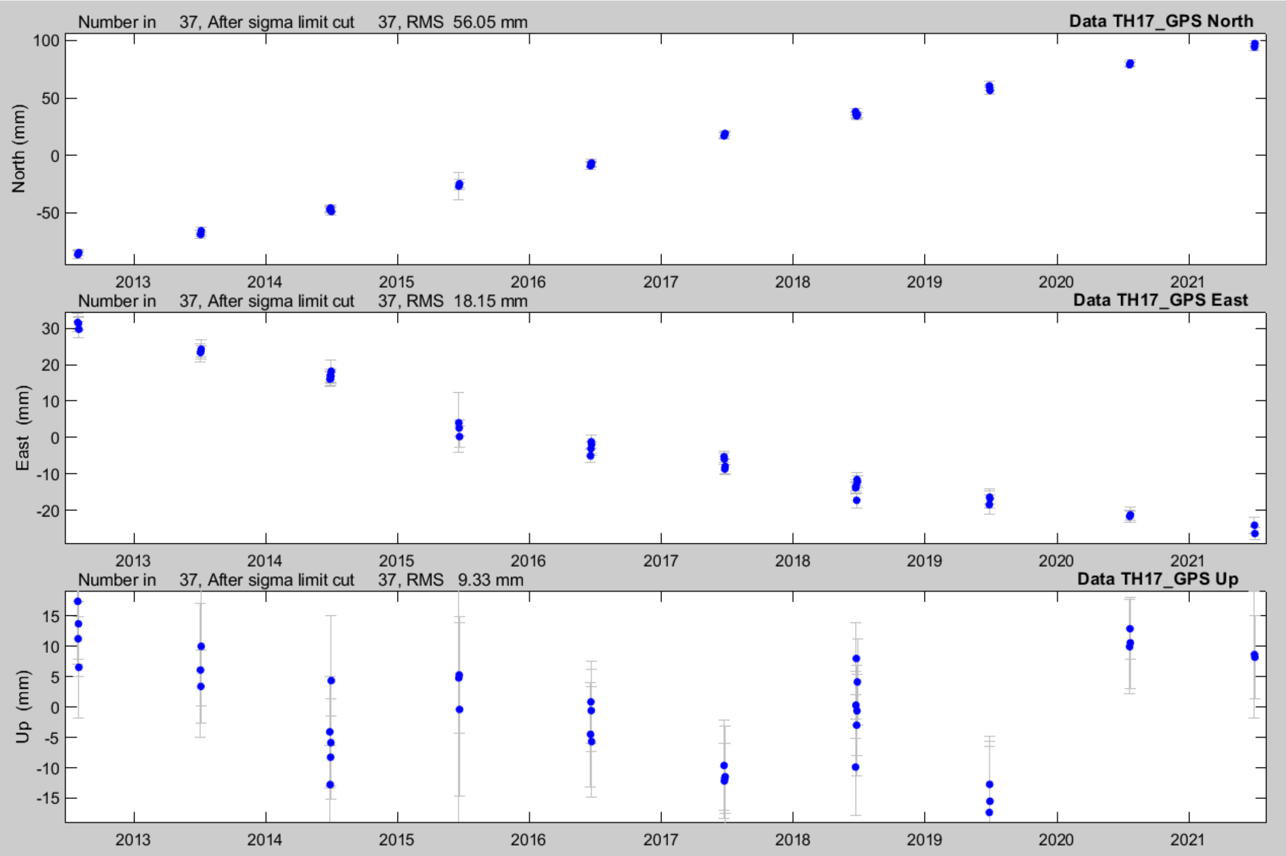

Figure 17. GNSS time series for TH17 station at Þeistareykir.

3. Velocity fields

3.1 Krafla and Námafjall areas

The previous chapter with time series of displacement at GNSS sites gives an indication of the temporal evolution of deformation at Krafla caldera. GNSS can also give an indication of the spatial pattern of deformation. For this purpose, we evaluate ground surface velocity fields based on the GNSS data collected in different campaigns through the past few years. Here, the GPS velocities evaluation has been made relative to stable Eurasian plate. The GPS velocities are showing the mean deformation rates accounting for the time periods 2015-2018, 2018-2020 or 2018-2021. Horizontal velocities for 2018-2021 (Figure 18) show 9-11 mm/yr (95% confidence interval) westnorth-west motion due to the location of the study area near the central axis of the plate boundary of the North American – Eurasian plate boundary (Drouin et al., 2017). The velocity field shows anomalies at some stations which are moving slightly different from the overall westnorth-west motion of most stations. One area is located near the Bjarnarflag Power Plant and one in the middle of the Krafla caldera. These differences are generally caused by sources of subsurface contraction/expansion at different depth located between the velocity anomalies. In the Krafla case, they relate to the pressure increase recorded in the Leirbotnar geothermal field in 2018 and 2019 (Hersir et al., 2020).

The overall vertical velocities 2018-2021 (Figure 19) show a general uplift with most of the higher values located inside the caldera. The effect of the glacial isostatic adjustment due to retreat of ice caps can account for 4-5 mm/yr of the regional uplift rate (Árnadóttir et al., 2009; Auriac et al., 2013; Drouin et al., 2017).

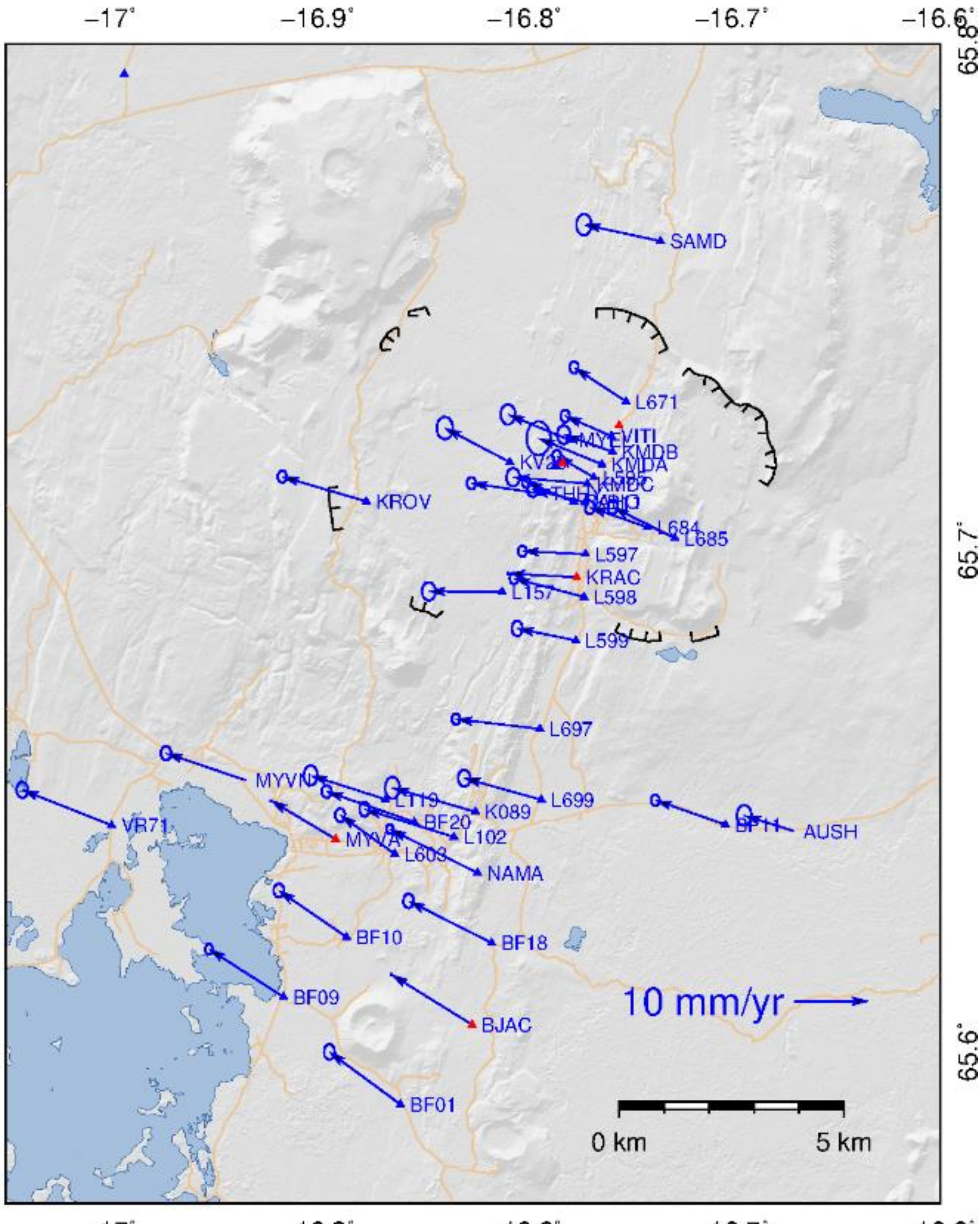

Figure 18. 2018-2021 horizontal GNSS velocities relative to the stable Eurasian plate, in the Krafla and Námafjall areas. Blue triangles show the campaign GNSS stations, while the red ones show the continuous stations. Ellipses indicate velocity uncertainties.

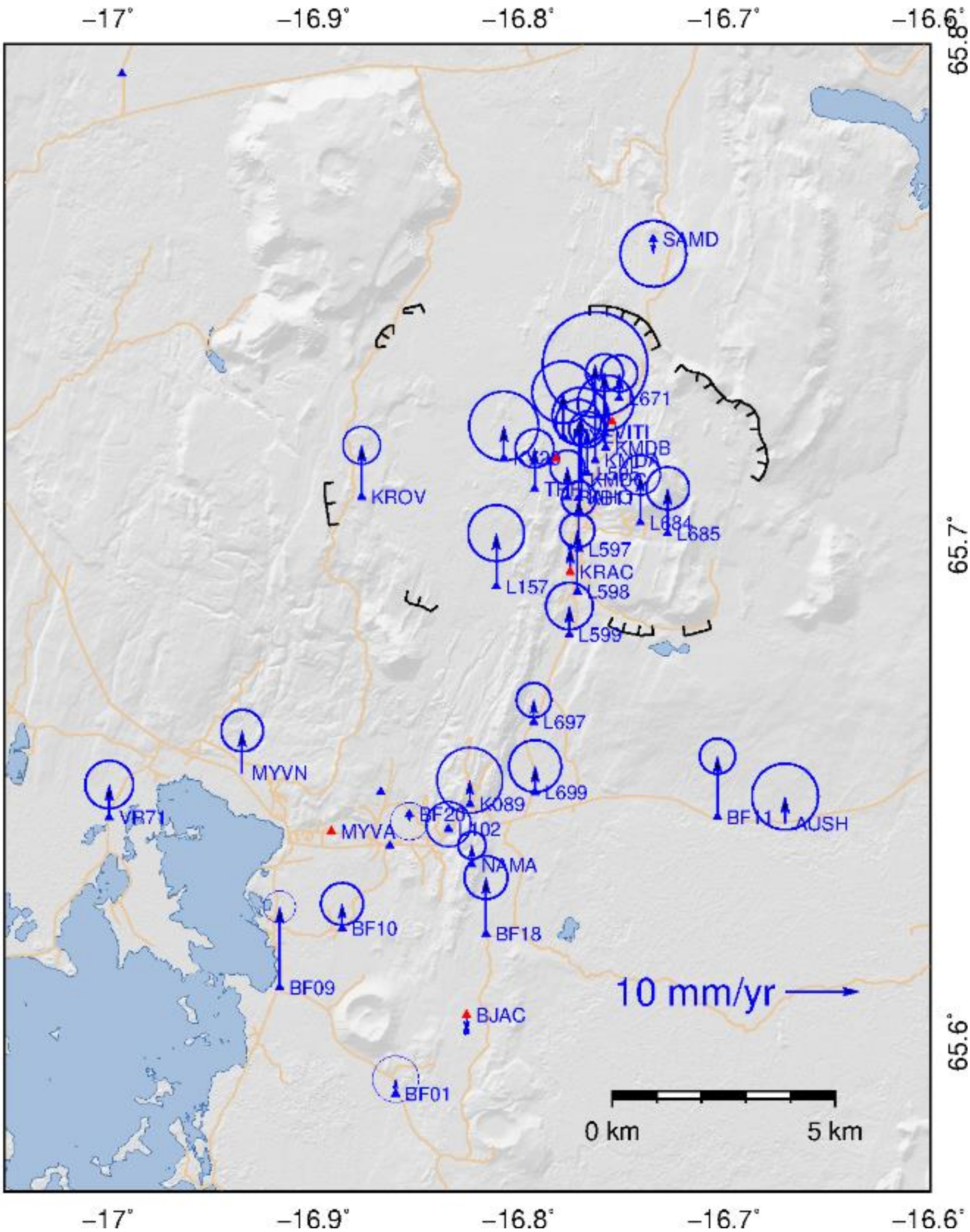

Figure 19. 2018-2021 Vertical (right) GNSS velocities in the Krafla and Námafjall areas. Blue triangles show the campaign GNSS stations, while the red ones show the continuous stations. Ellipses indicate velocity uncertainties.

We use the GNSS observations to give a more complete indication of the spatial changes through time. For this purpose, we compared the difference velocity fields for 2015-2018 and 2018-2020, as well as the difference velocity fields between 2015-2018 and 2018-2021. We evaluated them for the GNSS stations with the most complete data in the 2015 – 2021 period. This approach allows us to isolate the signal due to changes in 2018, although is implicit the assumption that any other deformation processes remain constant between the two periods.

The horizontal difference velocity field for 2015-2018 and 2018-2020 (Figure 20) reveals an inflation pattern within the Krafla caldera, witnessed as general horizontal movement away from an area located in the middle of the caldera. The amount of the horizontal displacement is highest for the GNSS stations in the central area of the caldera, with average rate 4.7 ± 1.9 mm/yr for the interval 2018-2020. If we include the 2021 measurements (Figure 22) the average velocity is 4.8 ± 2.5 mm/yr. The amount of the horizontal displacement is highest for the GNSS stations in the central area of the caldera and decrease in the stations near or outside the southern caldera boundaries.

The vertical difference velocity field pattern for 2018-2020 (Figure 21) shows uplift for all the stations inside the caldera, except for L685 station in the south-east part, together with L599 and L697 GNSS stations, outside the caldera boundaries. These stations show subsidence, but the deformation pattern show uplift for the difference velocity 2018-2021 (Figure 23).

Figure 24 shows a comparison between the two velocity differences evaluated for both the horizontal and vertical motion.

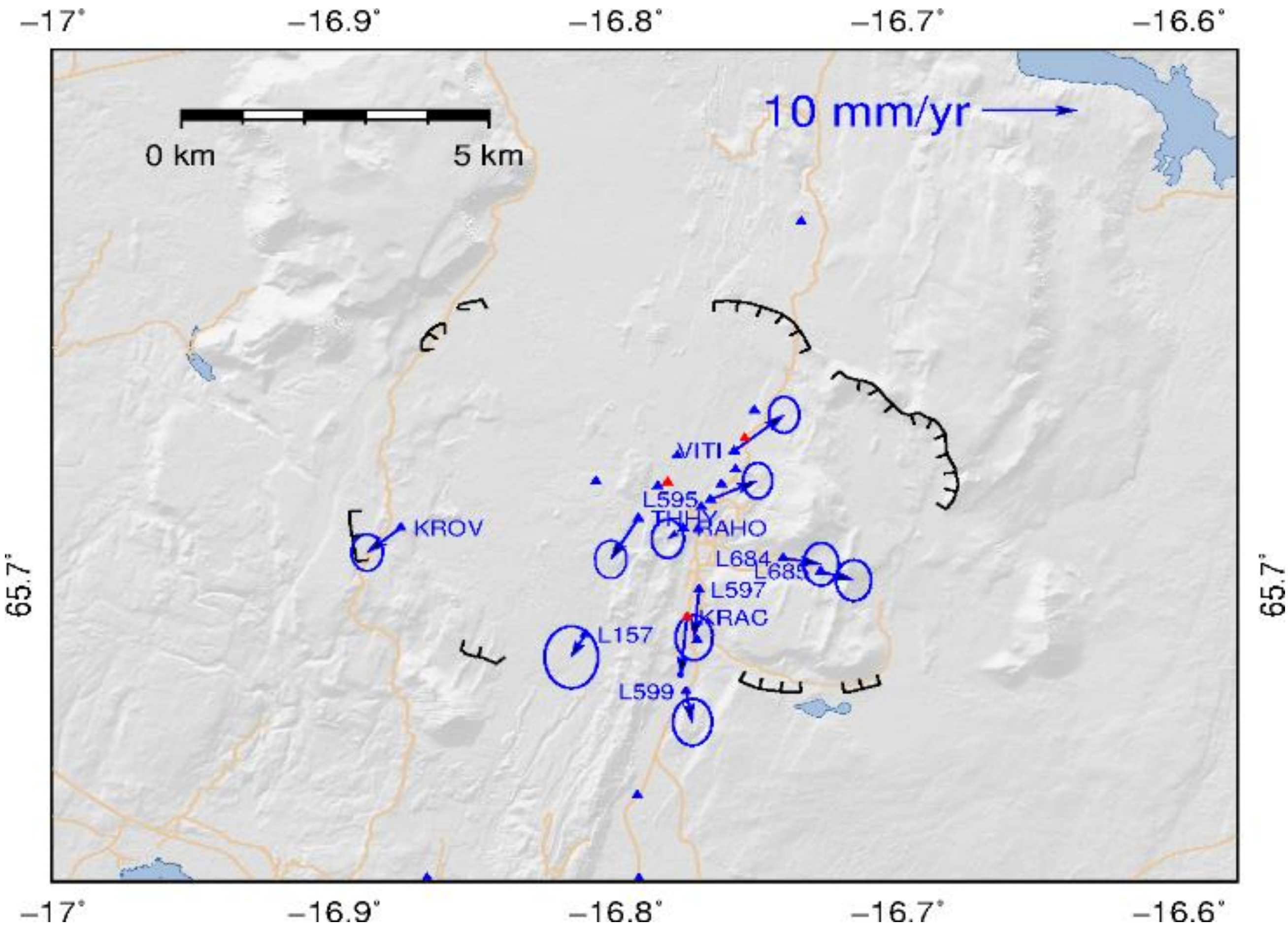

Figure 20. Horizontal difference velocity field 2018-2020 relative to 2015-2018 in the Krafla area. Blue triangles show the campaign GNSS station, while the red ones show the continuous station. Ellipses indicate velocity uncertainties.

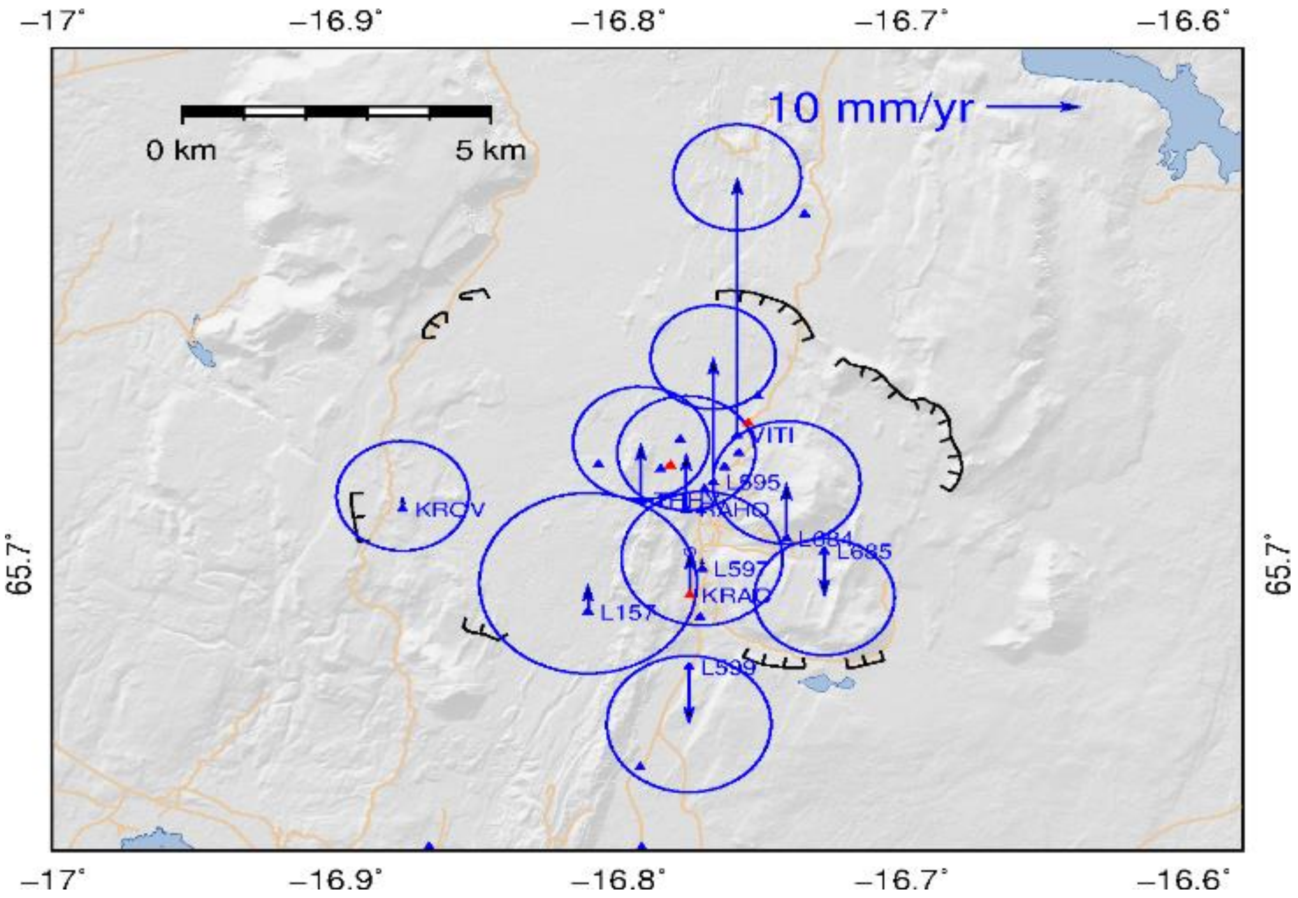

Figure 21. Vertical difference velocity field 2018-2020 relative to 2015-2018 in the Krafla area. Blue triangles show the campaign GNSS station, while the red ones show the continuous station. Ellipses indicate velocity uncertainties.

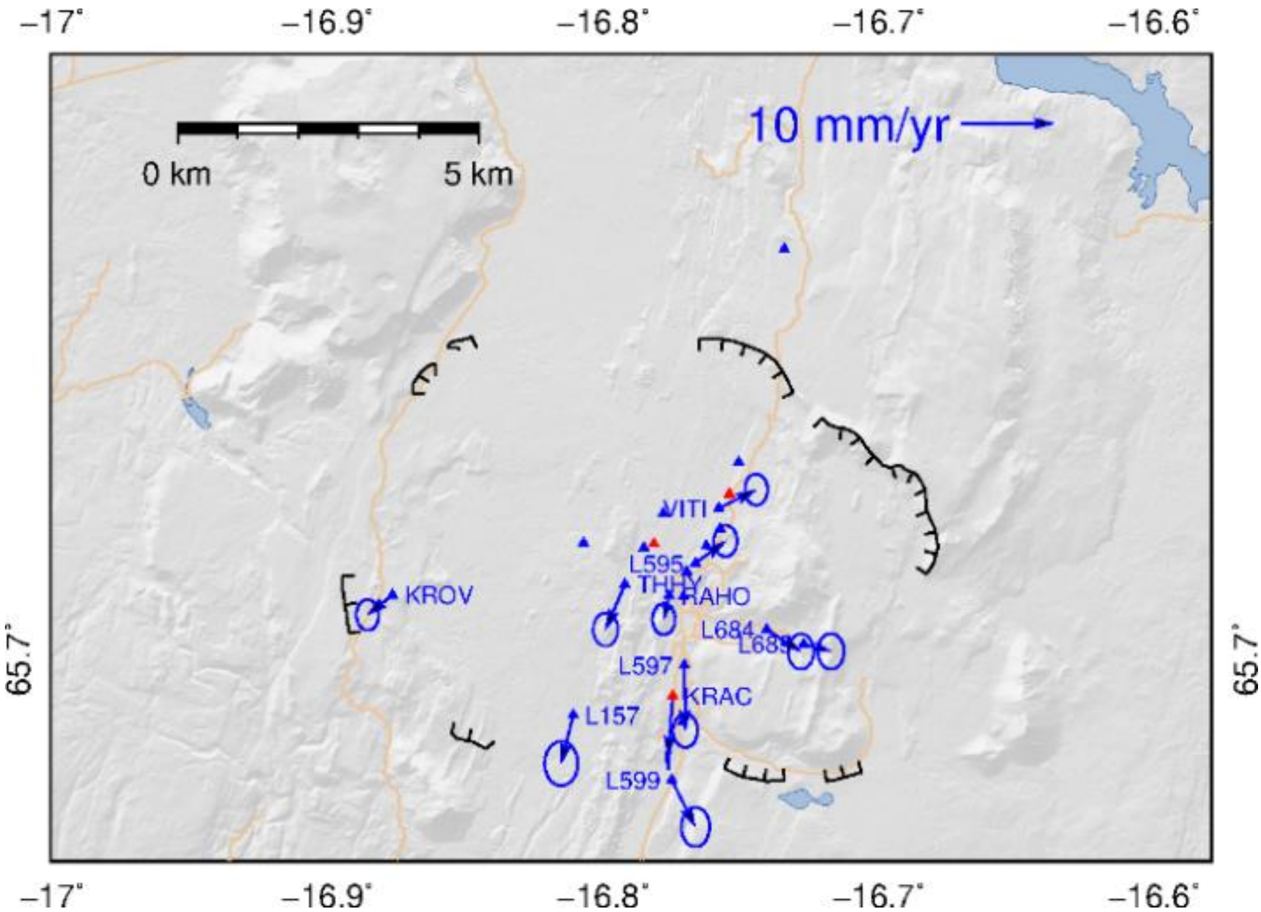

Figure 22. Horizontal difference velocity field 2018-2021 relative to 2015-2018 in the Krafla area. Blue triangles show the campaign GNSS station, while the red ones show the continuous station. Ellipses indicate velocity uncertainties.

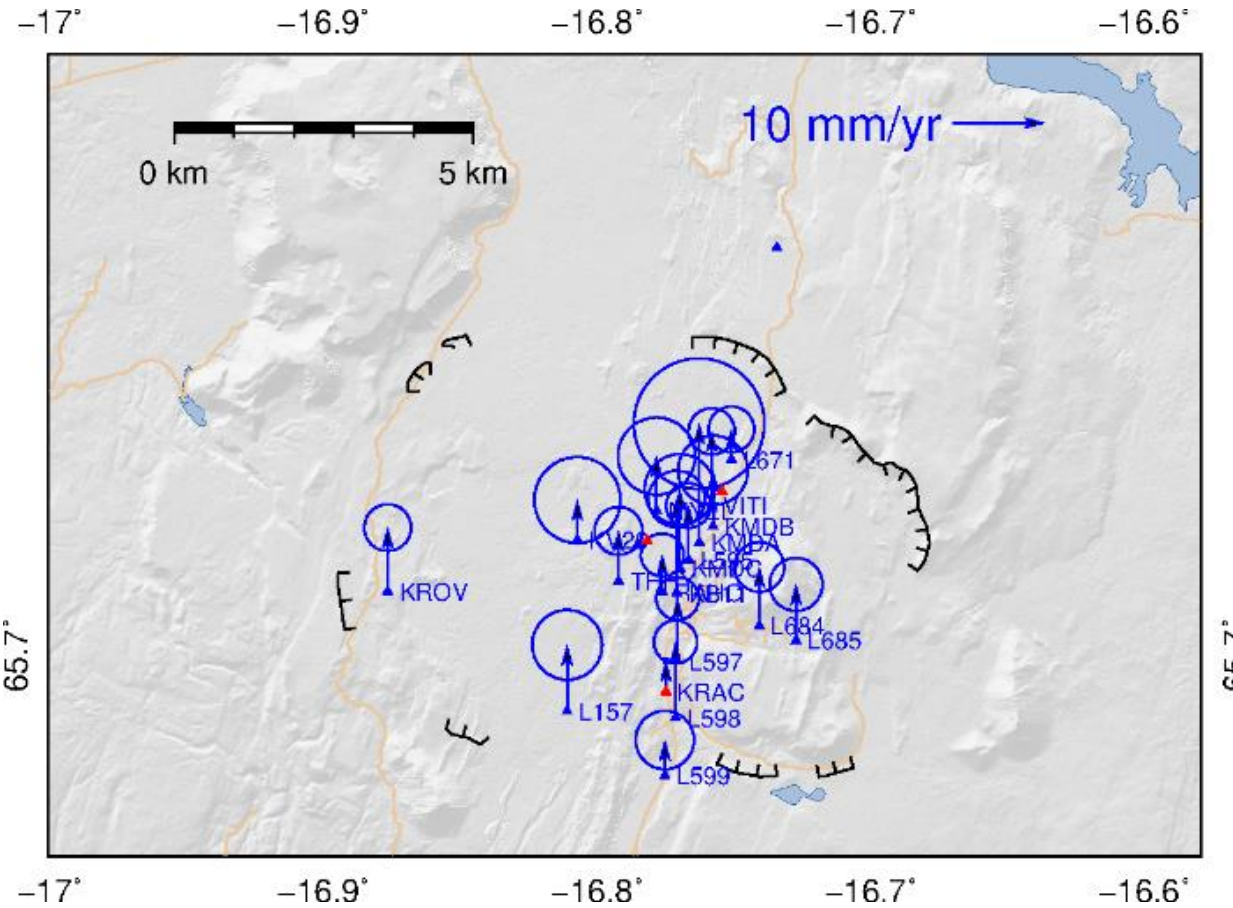

Figure 23. Vertical difference velocity field 2018-2021 relative to 2015-2018 in the Krafla area. Blue triangles show the campaign GNSS station, while the red ones show the continuous station. Ellipses indicate velocity uncertainties.

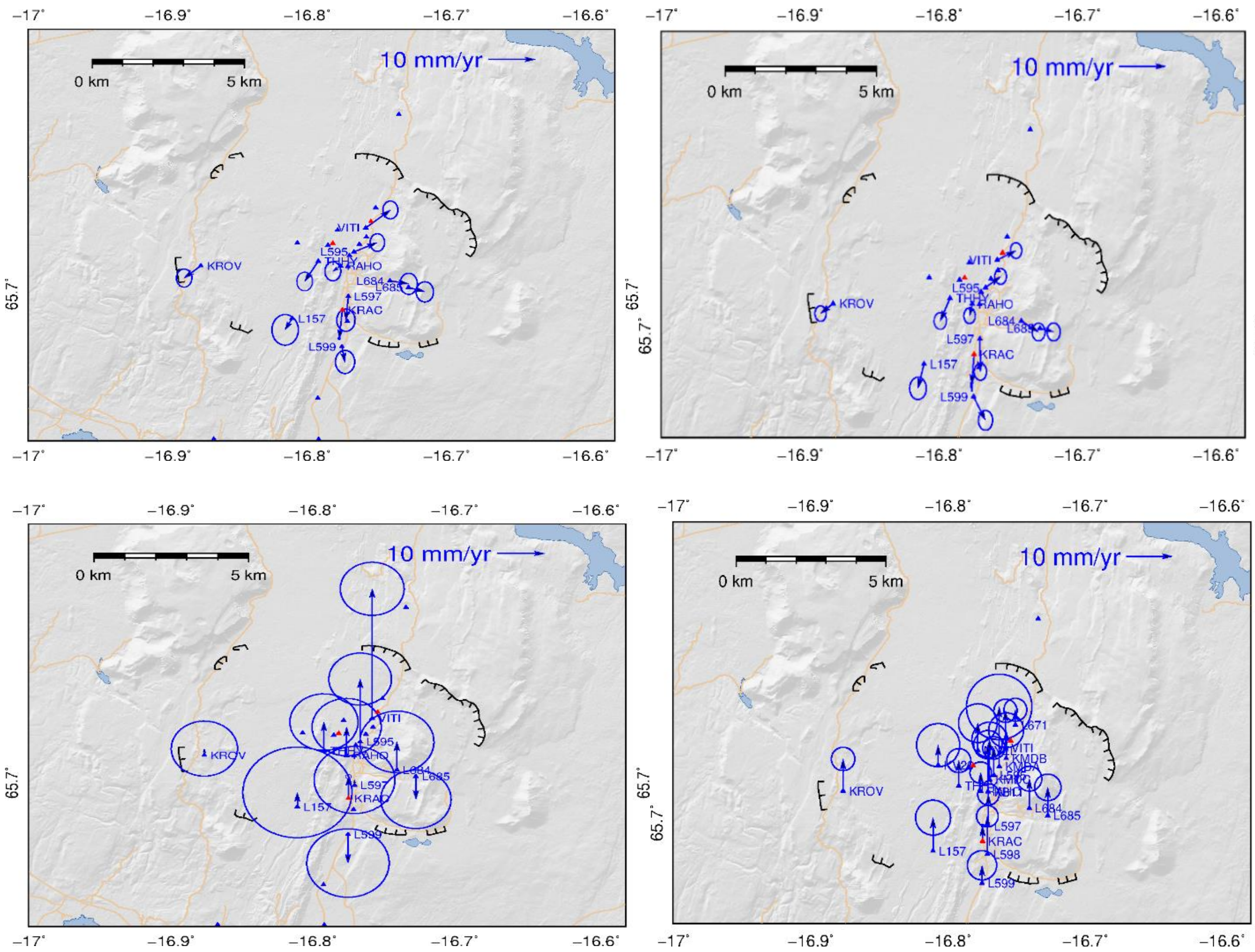

Figure 24. Horizontal (upper left panel) and vertical (lower left panel) difference velocity field 2018-2020 relative to 2015-2018 in the Krafla area. Horizontal (upper right panel) and vertical (lower right panel) difference velocity field 2018-2021 relative to 2015-2018 in the Krafla area. Blue triangles show the campaign GNSS station, while the red ones show the continuous station. Ellipses indicate velocity uncertainties (two-sigma).

3.2 Þeistareykir

As for Krafla, we apply here the same approach to create time difference velocity fields to study deformation at Þeistareykir area. The difference velocity field are obtained subtracting velocities in the time interval 2015-2017 from velocities in 2017-2021. The result gives the horizontal (Figure 25) and vertical (Figure 26) difference velocity field. The horizontal difference velocity field show a small signal for all the stations. Some of the GNSS stations (HITR, TR15 and THER), show a higher signal up to 2-3 mm/yr. The signal is displayed by few stations 1-2 km far from the north-west hills of Bæjarfjall and shows contraction.

The high values shown for vertical difference velocity fields (Figure 26) do not seem to be very reliable.

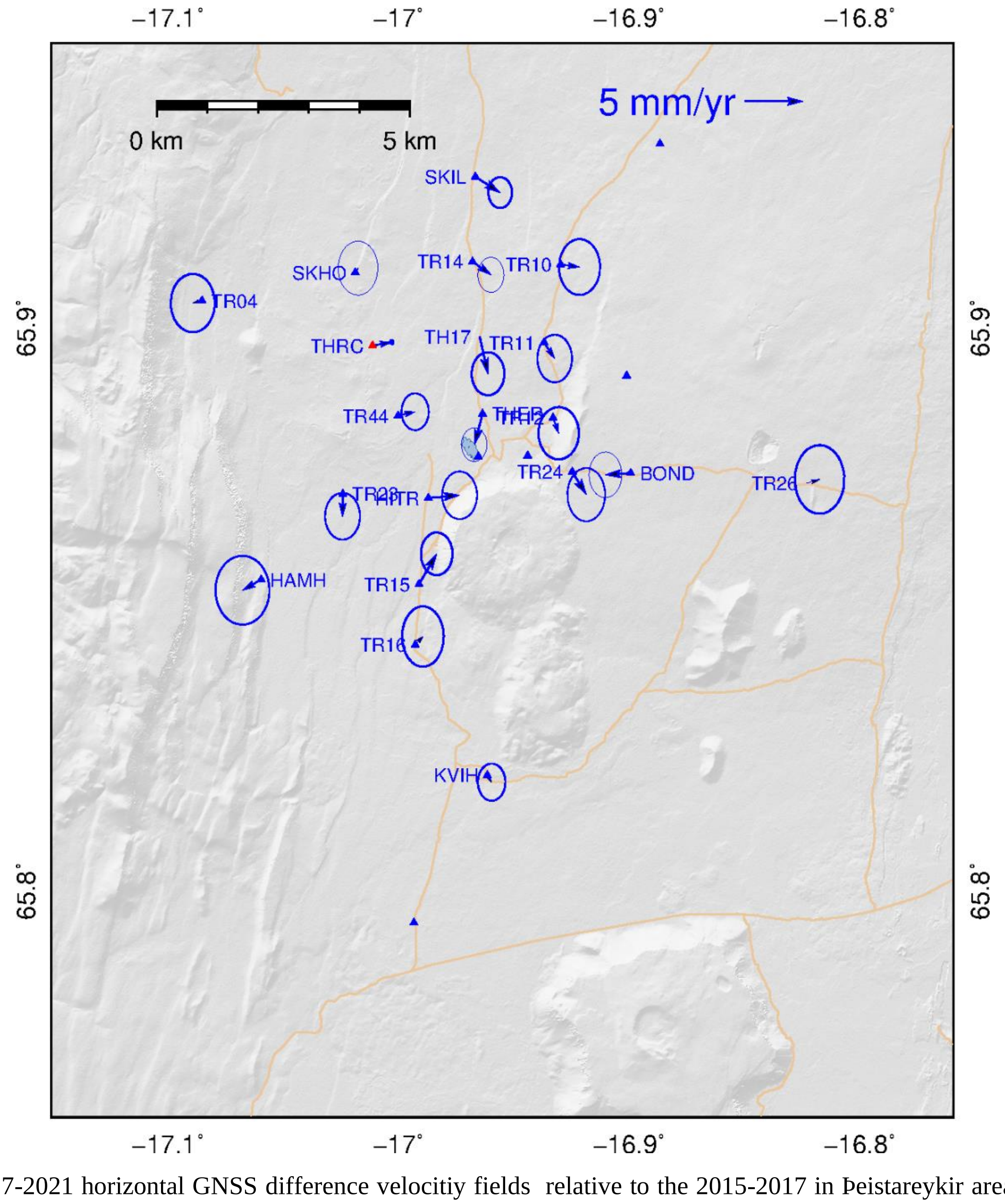

Figure 25. 2017-2021 horizontal GNSS difference velocitiy fields relative to the 2015-2017 in Þeistareykir area. Blue triangles show the campaign GNSS station, while the red ones show the continuous station.

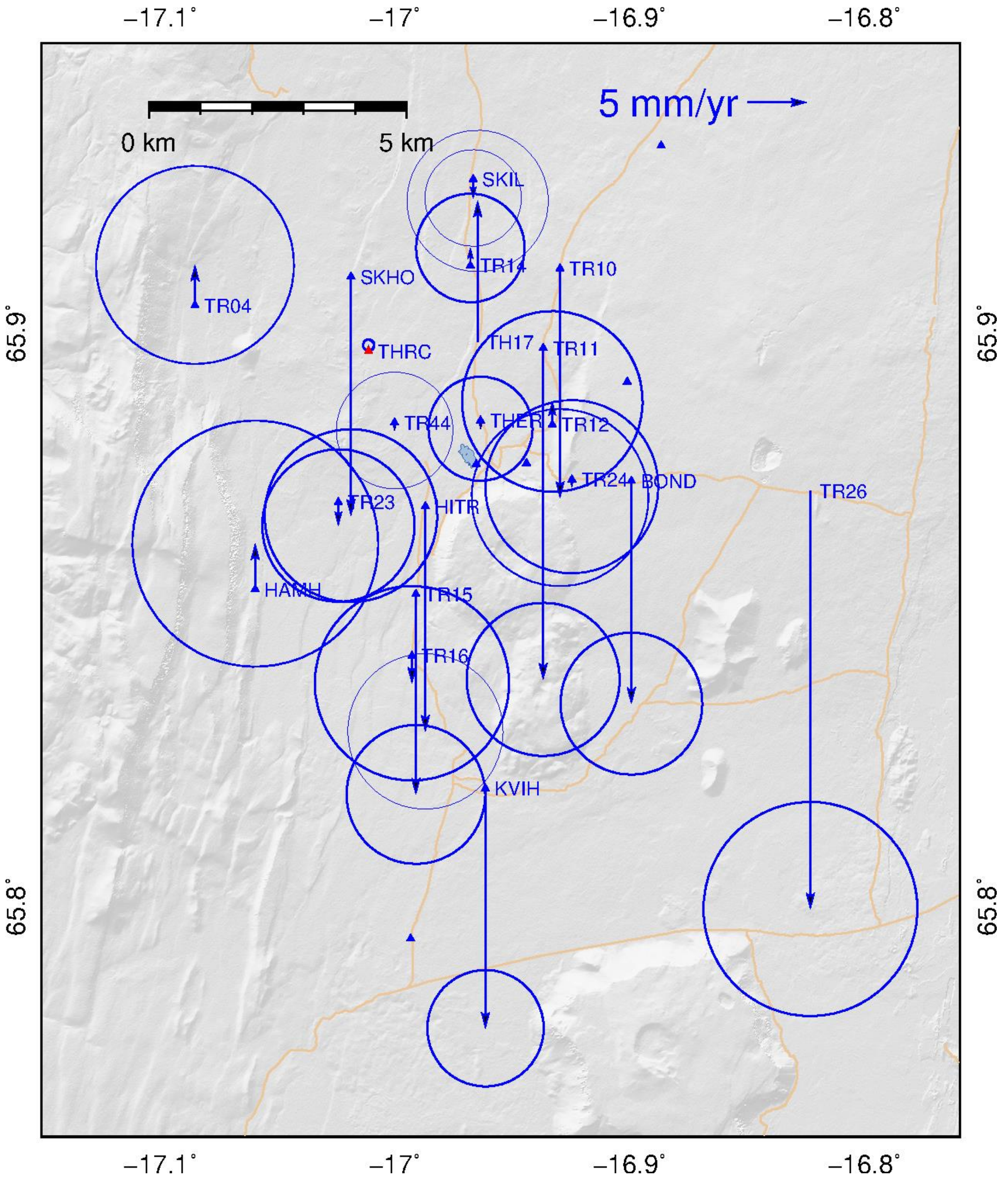

Figure 26. 2017-2021 vertical GNSS velocities relative to the 2015-2017 in Þeistareykir area. Blue triangles show the campaign GNSS station, while the red ones show the continuous station.

4. MODELLING

4.1 Krafla

The three-dimensional horizontal and vertical velocity difference fields (2018-2021 with respect to 2015-2018) have been used to model the deformation at Krafla. In the following modelling, we use the GNSS stations that have the most complete record from 2015 to 2021. We employ the open-source Geodetic Bayesian Inversion Software (GBIS, Bagnardi and Hooper, 2018), which allows to perform an inversion of GNSS data to estimate deformation source parameters with a Bayesian approach. We here assume that deformation is caused by a point source of pressure within a uniform elastic half-space, a Mogi source (Mogi, 1958) or by a sill-like deformation source (Okada, 1985). The modelling procedure estimates then the location and depth of the source and volume change associated with it for the point pressure source and, additionally, parameters like strike, opening, length and width for the sill source. The Bayesian approach for inverting the geodetic data finds probability density functions for each of the model parameters (Figures 27 and 28), and provides therefore a good estimate of model parameter uncertainties. The results are presented below in Tables 2 and 3.

For a point pressure source (sometimes referred to as a Mogi source), the modelling procedure estimates an optimal depth ~2.4 km (2.1– 2.8 km, 95% confidence interval) and a volume change ~4.3×10^5 m^3/yr (ranging from $3.4–5.8\cdot10^5$ m^3/yr). For a sill-like source, the inversion finds an optimal length of the sill around 6.4 km (5.0-9.7 km, 95% confidence interval) and width 135 m (106-187 m, 95% confidence interval) at depth ~ 2.2 km (1.8– 2.6 km, 95% confidence interval). The probability density functions are well constrained in the point pressure solution, while the sill source gives poor constrains for two parameters: width and opening. The sill inversion result gives an aspect ratio relatively high, showing how the sill seems to be shaped as a long and thin intrusion, if the sill is the correct model.

The resulting comparison between the observations (velocity data) and the model estimation are in broad agreement. Figures 29 and 30 shows the horizontal displacement with blue arrows being the data, red arrows the model estimation and yellow diamond is the inferred point pressure source location. Black bar in Figure 30 shows the location of the sill source in a map view.

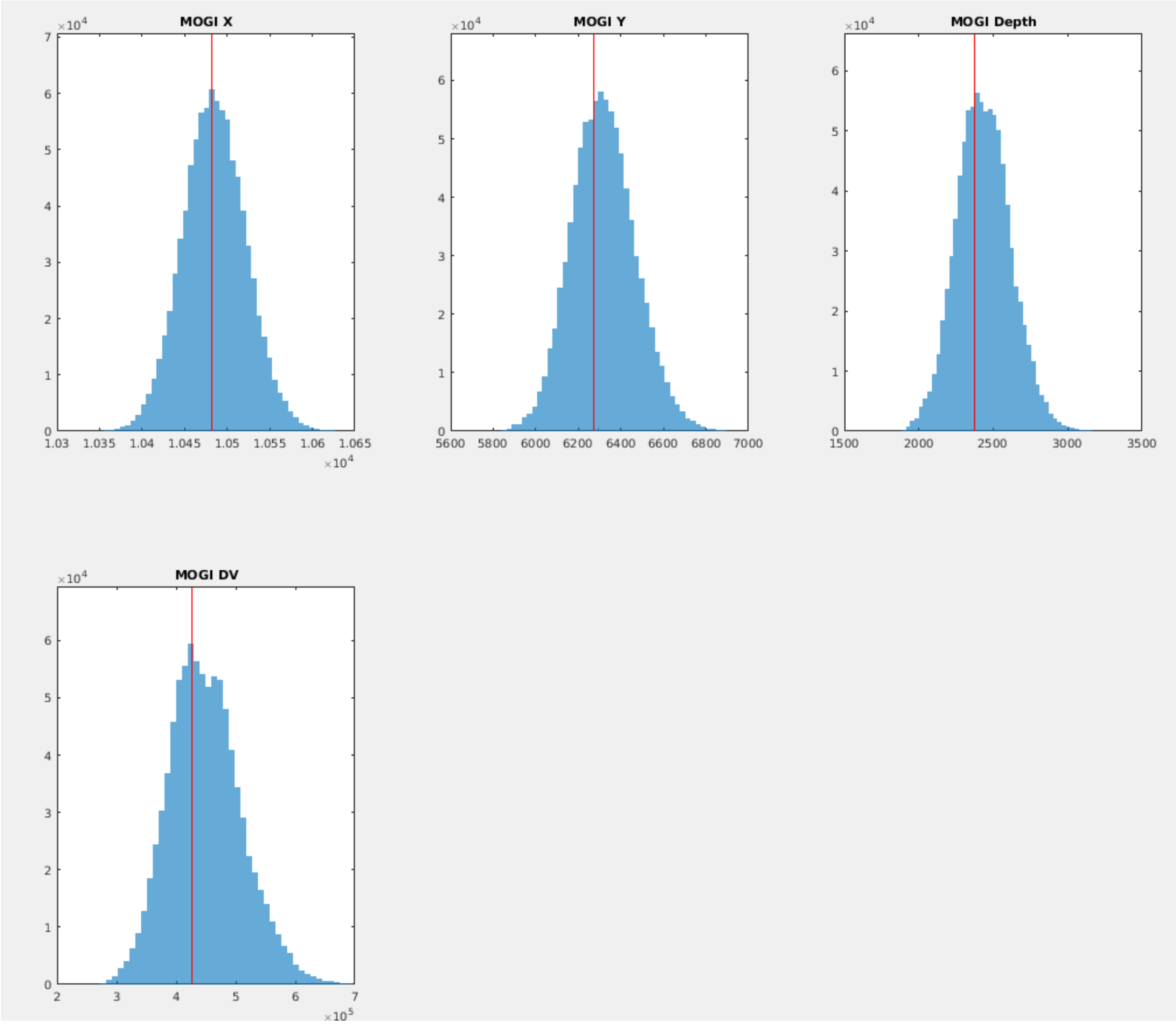

Figure 27. Inferred scaled probability density functions for point source model parameters. Red lines represent the optimal probability solution.

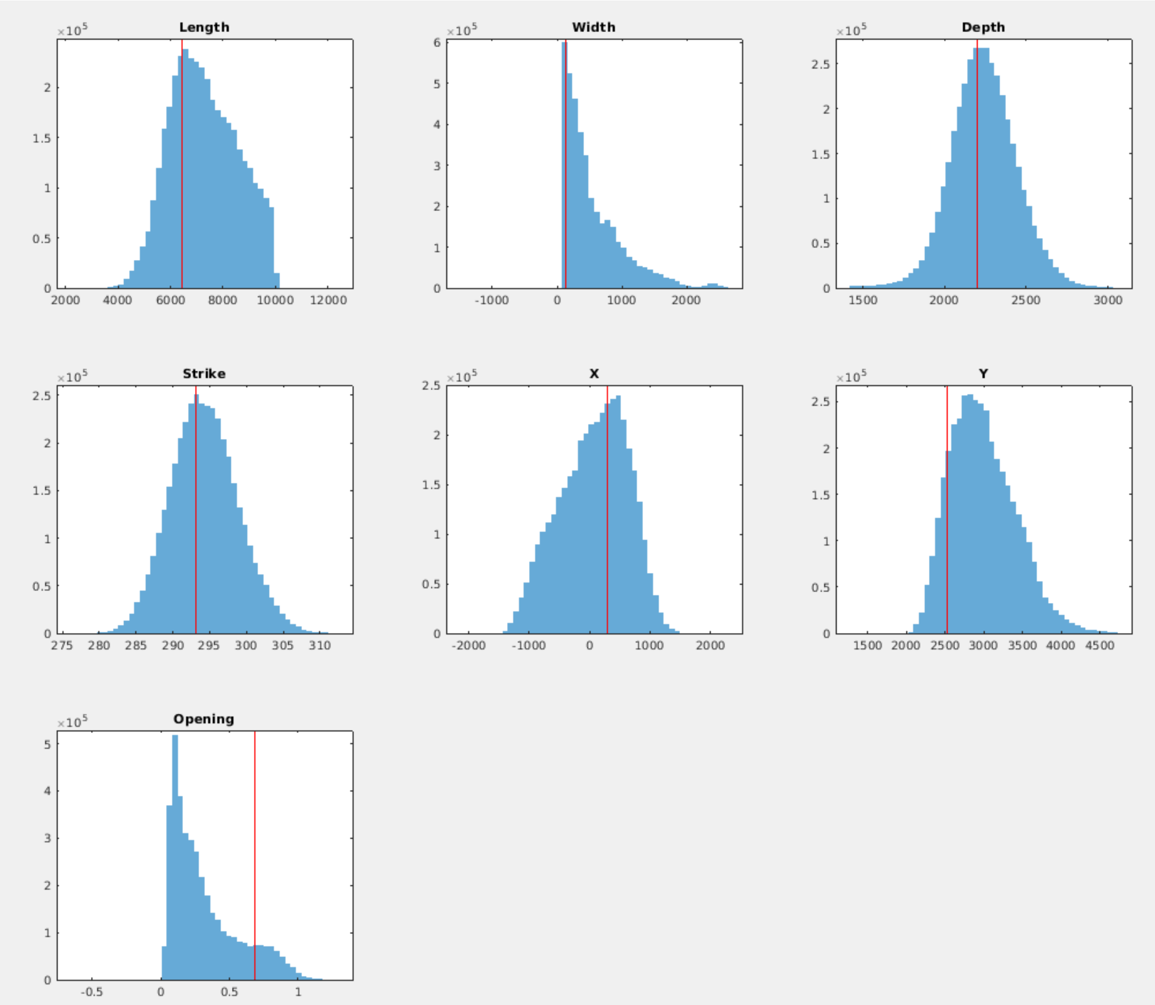

Figure 28. Inferred scaled probability density functions for geodetic sill-like model parameters. Red lines represent the optimal probability solution.

Table 2. Results from GBIS inversion of 2018-2021 and 2015-2018 difference velocity fields from GNSS. Depth in meters and volume in m^3/yr. Columns show model parameters, the optimal inversion result, and the 2.5 and 97.5 percentiles of posterior probability density functions. The range spanned by the 2.5 and 97.5 percentiles is the 95% confidence interval.

MODEL PARAM.	Optimal	2.5%	97.5%
MOGI longitude	-16.7713	-16.7728	-16.7696
MOGI latitude	65.71640	65.7143	65.7196
Depth (m)	2377	2092	2805

Volume change (m^3/yr)	426614	339668	580434

Table 3. Results from GBIS inversion of 2018-2021 and 2015-2018 difference velocity fields from GNSS for a sill-like source. Columns show model parameters, the optimal inversion result, and the 2.5 and 97.5 percentiles of posterior probability density functions. The range spanned by the 2.5 and 97.5 percentiles is the 95% confidence interval.

MODEL PARAMETERS	Optimal	2.5%	97.5%
Longitude	-16.80	-16.83	-16.78
Latitude	65.72	65.72	65.73
Length (m)	6446	5026	9750
Width (m)	135	106.7	1879
Depth (m)	2200	1845	2644
Opening (m)	0.69	0.05	0.90
Strike (degrees)	293	286	304

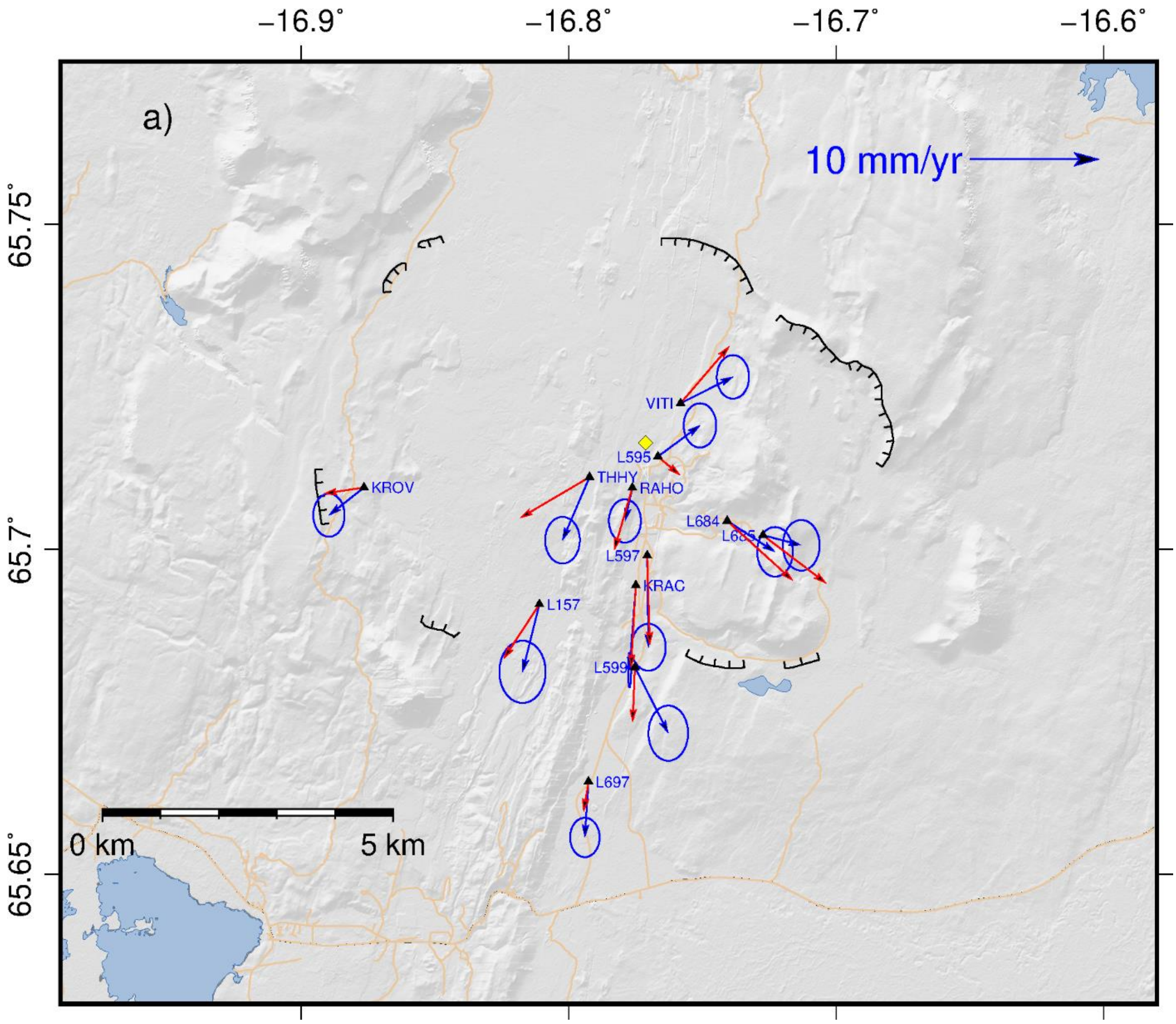

Figure 29. Comparison between GNSS horizonal data (blue) and predictions of a best fitting point source of pressure (Mogi) model (red). Yellow diamond is showing the source center location.

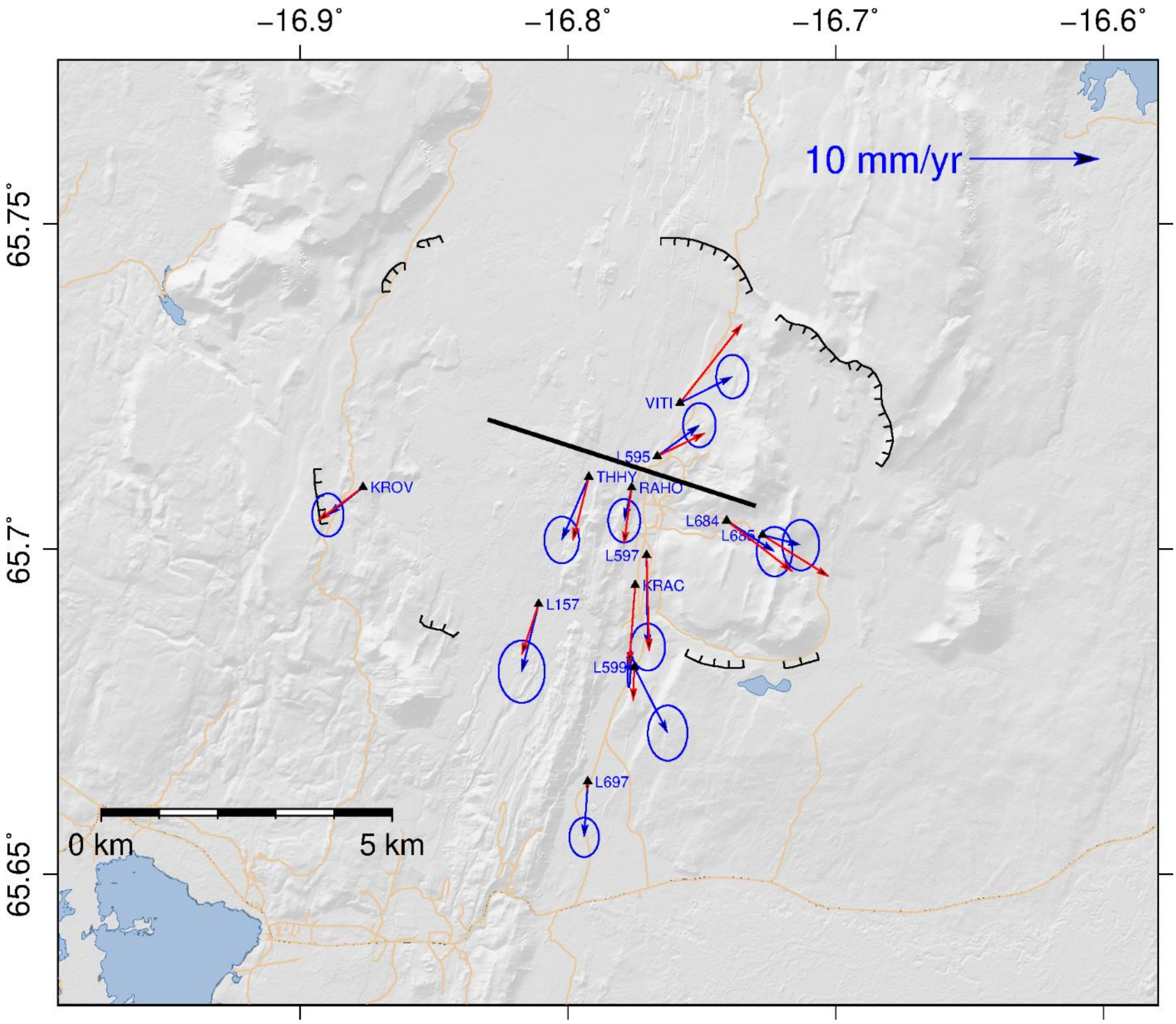

Figure 30. Comparison between GNSS horizonal data (blue) and predictions of a best fitting sill-like source (red).

To quantify the prediction capability of the models with different geometry, we considered the root-mean-square (RMS) value of residuals between observations and model predications, according to the following formula:

$$RMS = \sqrt{\frac{\sum((dobs - dpre)/ObsUncer)^2}{N}} \quad (1)$$

where d_{obs} are observation data, d_{pre}, are predicted displacement from a model, *ObsUncer,* are the observation uncertainties and *N* is the number of observations (N=12 for the vertical component and N=24 for the horizontal -east and north- components). These values can be compared to the RMS of the observations themselves (equation 1 with predicted displacements equal to zero).

For the Mogi and sill-like models presented above, the RMS value estimated is lower than the RMS estimated for GNSS data without a model (Table 4). The Mogi solution has a significantly lower RMS value for both the vertical and horizontal displacement and is thus our preferred solution.

Table 4. RMS values for observations (GNSS observations) and the different model predictions .

RMS	GNSS observations (mm/yr)	Mogi source (mm/yr)	Sill-like source (mm/yr)
Horizontal displacement	2.02	0.62	0.79
Vertical displacement	4.72	0.98	1.77

Here we have presented the results obtained by modelling the GNSS difference velocity field 2018-2021. When compared to earlier modelling results, which consider GNSS and InSAR difference velocity fields in the interval 2018-2020 (Mogi model; volume change (2.7-3.8)$\times 10^5$ m^3/yr; 95% confidence interval), the GNSS difference velocity field 2018-2021 reveals slightly larger volume change ((3.4-5.8) $\times 10^5$ m^3/yr; 95% confidence interval). Such result agrees with that the deformation process is still ongoing in 2021, at comparable depth as before. However, it has to considered that the 95% confidence intervals overlap. Also, that in the modelling procedure for 2021, we did not include the InSAR data. Further attempt to include the InSAR difference velocity field to 2021 could offer a better constraint for the source parameters.

4.2 Þeistareykir

We used the same modelling approach as in paragraph 4.1. The three-dimensional velocity difference fields (2017-2021 with respect to 2015-2017) have been used to model the deformation at Þeistareykir. In the modelling, we use the GNSS stations that have the most complete record from 2015 to 2021, in the area near Bæjarfjöll. We employ the open-source GBIS software to perform an inversion of GNSS data for a point pressure source, a sill geometry, and a fault model.

The modelling did not find a solution that can explain the data. Most of the parameters were poorly constraint and did not converge to a particular value. These results highlight the small signal displayed by the velocity fields, with no particular pattern detected

5. REFERENCES

Altamimi, Z., Métivier, L., and Collilieux, X. (2012*).* ITRF2008 plate motion model. *Journal of Geophysical Research: Solid Earth, 117(B7).*

Árnadóttir, T., B. Lund, W. Jiang, H. Geirsson, H. Björnsson, and P. Einarsson (2009), Glacial rebound and plate spreading: Results from the first countrywide GPS observations in Iceland, *Geophys. J. Int.*, *177*, 691–716, doi:10.1111/j.1365-246X.2008.04059.x.

Auriac, A. (2014), Solid Earth response to ice retreat and glacial surges in Iceland inferred from satellite radar interferometry and finite element modelling, PhD thesis, Faculty of Earth Sciences, Univ. of Iceland.

Bagnardi, M. and Hooper, A. (2018). Inversion of surface deformation data for rapid estimates of source parameters and uncertainties: A Bayesian approach. *Geochemistry, Geophysics, Geosystems*, *19.*

Herring, T. and McClusky, S. (2009). *GAMIT/GLOBK MATLAB TOOLS.* From: http://wwwgpsg.mit.edu/~tah/GGMatlab/#_tsview

Herring, T., R. King, and S. McClusky (2010). *Introduction to gamit/globk, Mas- sachusetts.* Institute of Technology, Cambridge, Massachusetts. https://geo.gob.bo/portal/IMG/pdf/intro_gg_1_.pdf

Hersir, G. P., Freysteinn Sigmundsson, Kristján Ágústsson, Ingvar Þór Magnússon, Vincent Drouin, Arnar Már Vilhjálmsson, Chiara Lanzi, Siqi Li, Halldór Geirsson and Sigrún Hreinsdóttir, Geodetic observation and surface deformation at Krafla in late 2019-2020, joint report: Landsvirkjun LV-2020-036; ÍSOR-2020/037; Science Institute University of Iceland report RH-9-20.

Lyard, F., Lefevre, F., Letellier, T. and Francis, O. (2006). Modelling the global oceantides: modern insights from FES2004. Ocean Dynamics, 56, 394–415.

Mogi, K. (1958), Relations between the eruptions of various volcanoes and the deformations of the ground surface around them, *Bull. Earthquake Res. Inst. Univ. Tokyo*, 36, 99–134.

Okada, Yoshimitsu. (1985). Surface deformation to shear and tensile faults in a halfspace. Bulletin of the Seismological Society of America. 75.

Zumberge, J. F.; Heflin, M. B.; Jefferson, D. C.; Watkins, M. M.; Webb, F. H. "Precise Point Positioning for the Efficient and Robust Analysis of GPS Data from Large Networks." Journal of Geophysical Research 102 (1997): 5005-5017.

Appendix A. 2021 GPS coordinates. Latitude and longitude are in decimal degrees from GAMIT-GLOBK processing. Latitude and Longitude for LHNC and SPBC are approximate decimal degree.

Longitude	**Latidute**	**Site name**
Continuous site		
-16,77491	65,6945	KRAC
-16,82537	65,60531	BJAC
-17,01134	65,89677	THRC
-16,89135	65,64232	MYVA
-16,75439	65,72465	SPBC
-16,781793	65,71723	LHNC
Campaign site		
-16,70311	65,6452	BF11
-16,72736	65,7022	L685
-16,73146	65,06004	A404
-16,7344	65,76125	SAMD
-16,74075	65,70442	L684
-16,75818	65,72252	VITI
-16,76277	65,71693	KMDA
-16,76667	65,71432	L595
-16,76982	65,71308	KMDC
-16,77063	65,69909	L597
-16,77096	65,70934	KB11
-16,77528	65,68188	L599
-16,77623	65,70951	RAHO
-16,79194	65,65019	L699
-16,79222	65,71114	THHY
-16,79263	65,66428	L697
-16,81096	65,69158	L157
-16,81598	65,62167	BF18
-16,8228	65,6356	NAMA
-16,82309	65,8724	TR26
-16,82383	65,64778	K089
-16,83421	65,6428	L102
-16,84322	65,79558	TR32
-16,85327	65,64572	BF20
-16,85994	65,58941	BF01
-16,86282	65,63938	L603
-16,86724	65,65027	L119
-16,87658	65,70956	KROV
-16,87685	65,96293	BLAS
-16,88611	65,62281	BF10

-16,89934	65,8742	BOND
-16,91656	65,61088	BF09
-16,92473	65,87443	TR24
-16,92597	65,79237	TR34
-16,92977	65,91115	TR10
-16,93304	65,88398	TR12
-16,9348	65,65405	MYVN
-16,93696	65,89731	TR11
-16,96151	65,82058	KVIH
-16,96364	65,88471	THER
-16,96486	65,89834	TH17
-16,96677	65,92666	SKIL
-16,96796	65,91166	TR14
-16,97372	65,95851	RAUH
-16,9871	65,86978	HITR
-16,99117	65,8545	TR15
-16,99284	65,84372	TR16
-16,99341	65,79436	RAND
-16,99965	65,6451	VR71
-17,00022	65,88436	TR44
-17,01884	65,90973	SKHO
-17,0242	65,87048	TR23
-17,04041	65,96203	HELL
-17,05198	65,72274	TR41
-17,08527	65,90475	TR04
-17,14863	65,96841	HOVA

Appendix B. Measurement of antenna slant height.

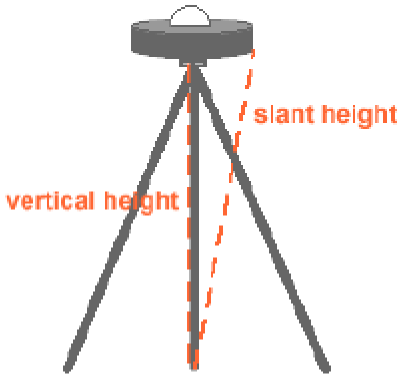

Slant height: Measure of the slope distance from the iron mark on the ground to the bottom of the antenna ground planes. The measurements are taken at least in three different sectors of the antenna, at the beginning and at the end of the survey, in meters and feet.

Appendix C. Example of the logsheet used during the setup of the instruments.

HÁSKÓLI ÍSLANDS

GPS Logsheet

CAMP: ____________

Monument Drawing:

SITE NAME:______________________________ SITE ID:___________

Monument Inscription:____

Location:____

Type of Monument:____

Operator(s):____

Institution(s):____

Receiver Type:___________________________

Receiver P/N:________________________________

Receiver S/N:________________________________

Receiver ID:_________________________________

Firmware version:____________________________

Sampling Int.: ____sec. Elev. Mask: ______°

Start Date:_____________________ DOY______

Start Time (UTC):_________

Stop Date:_____________________ DOY______

Stop Time (UTC):_________

Antenna Type:_______________________________

Antenna P/N:________________________________

Antenna S/N:________________________________

Antenna ID:_________________________________

Alignment:

☐ Magnetic North

☐ True North

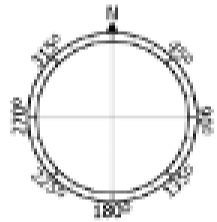

Magn. Decl.:________

Comp. Reading:_______

Level: Start? ______ Stop?_______________

Centered: Start?______ Stop?_______________

Height: Type: ☐ Vertical ☐ Slant

Read from: ☐ Bottom ☐ Top

Tripod: ☐

#	Start Height	Stop Height

Slant height in feet:___________

Average Slant Height: ___________m

Corrected vertical height: ___________m

☐ Spike Mount: Fixed Height: __________m

☐ Vertical Mount: Fixed Height:__________m

☐ Other: ______________ Height:__________m

Comments:

May 2011